

## 2 A Smooth Finite Element Method Based on Reproducing 3 Kernel DMS-Splines

4 Sunilkumar N<sup>1</sup> and D Roy<sup>1,2</sup>

5 **Abstract:** The element-based piecewise smooth functional approximation in the  
6 conventional finite element method (FEM) results in discontinuous first and higher  
7 order derivatives across element boundaries. Despite the significant advantages of  
8 the FEM in modelling complicated geometries, a motivation in developing mesh-  
9 free methods has been the ease with which higher order globally smooth shape  
10 functions can be derived via the reproduction of polynomials. There is thus a case  
11 for combining these advantages in a so-called hybrid scheme or a ‘smooth FEM’  
12 that, whilst retaining the popular mesh-based discretization, obtains shape func-  
13 tions with uniform  $C^p$  ( $p \geq 1$ ) continuity. One such recent attempt, a NURBS based  
14 parametric bridging method (Shaw *et al.* 2008b), uses polynomial reproducing,  
15 tensor-product non-uniform rational B-splines (NURBS) over a typical FE mesh  
16 and relies upon a (possibly piecewise) bijective geometric map between the physi-  
17 cal domain and a rectangular (cuboidal) parametric domain. The present work aims  
18 at a significant extension and improvement of this concept by replacing NURBS  
19 with DMS-splines (say, of degree  $n > 0$ ) that are defined over triangles and provide  
20  $C^{n-1}$  continuity across the triangle edges. This relieves the need for a geometric  
21 map that could precipitate ill-conditioning of the discretized equations. Delau-  
22 nay triangulation is used to discretize the physical domain and shape functions are  
23 constructed via the polynomial reproduction condition, which quite remarkably re-  
24 lieves the solution of its sensitive dependence on the selected knotsets. Derivatives  
25 of shape functions are also constructed based on the principle of reproduction of  
26 derivatives of polynomials (Shaw and Roy 2008a). Within the present scheme, the  
27 triangles also serve as background integration cells in weak formulations thereby  
28 overcoming non-conformability issues. Numerical examples involving the evalua-  
29 tion of derivatives of targeted functions up to the fourth order and applications of  
30 the method to a few boundary value problems of general interest in solid mechan-  
31 ics over (non-simply connected) bounded domains in 2D are presented towards the

---

<sup>1</sup> Structures Lab, Department of Civil Engineering, Indian Institute of Science, Bangalore 560012, India

<sup>2</sup> Communicating author; Email: royd@civil.iisc.ernet.in

32 end of the paper.

33 **Keywords:** DMS-splines, Delaunay triangulation; globally smooth shape func-  
34 tions; polynomial reproduction; boundary value problems.

## 35 1 Introduction

36 Numerical solutions of models of complex engineering structures often pose chal-  
37 lenges that include appropriate treatment of nonlinearity of various forms, the com-  
38 plicated domain geometry and the boundary. The most popular approximation, the  
39 finite element method (FEM), employs an element-based discretization of the spa-  
40 tial domain, which is a key feature as element-wise approximations of field vari-  
41 ables not only provide a relief from the search of globally admissible functions,  
42 but also introduces versatility in approximating complex geometries with the ac-  
43 curacy of approximation generally increasing with decreasing element sizes. The  
44 governing equations are often solved through an element-wise application of the  
45 variational or Galerkin method (symmetric, unsymmetric or discontinuous), where  
46 the interpolating trial and test functions are piecewise polynomials over elements,  
47 thereby attaining at best  $C^0$  continuity. Achieving  $C^1$  or higher order global conti-  
48 nuity uniformly in the domain interior is however a non-trivial problem, especially  
49 in 2D or still higher dimensional domains, and an efficient solution to this problem  
50 remains mostly elusive.

51 Use of a conventional element-based discretization has its other pitfalls as well. For  
52 instance, repeated interactions with the CAD during mesh refinement are a costly  
53 procedure. Then, in large deformation problems, solutions may get affected due to  
54 element distortions. Moreover, as the continuum is assumed to be connected, it is  
55 difficult to model a possible fracture of the material body into a number of pieces. A  
56 way out of some of these drawbacks is possible with mesh-free methods, wherein  
57 the domain is discretized by a set of nodes (also called particles). Over the last  
58 two decades, researchers have shown keen interest in developing and expanding  
59 the realm of applications of mesh free methods. Some of these methods include  
60 the smooth particle hydrodynamics (SPH), (Lucy 1977; Gingold and Monaghan  
61 1977), the diffuse element method (DEM) (Nayroles *et al.* 1992), the element free  
62 Galerkin method (EFG) (Belytschko *et al.* 1994), the reproducing kernel particle  
63 method (RKPM) (Liu *et al.* 1995a, 1995b), Moving least square reproducing kernel  
64 (MLSRK) method (Liu *et al.* 1997), the partition of unity method (PUM) (Babuška  
65 and Melenk 1997), the  $h$ - $p$  Clouds (Duarte and Oden 1997), the mesh-free local  
66 boundary integral equation method (LBIE) (Zhu *et al.* 1998), the mesh-less local  
67 Petrov–Galerkin method (MLPG) (Atluri *et al.* 1999), error reproducing kernel  
68 method (ERKM) (Shaw and Roy 2007a), error reproducing and interpolating kernel

69 method (ERIKM) (Shaw *et al.* 2008c) and several others. However, these methods  
70 do not possess the versatility of element-based domain discretization.

71 Incidentally, most mesh-free methods are not strictly ‘mesh-free’, especially when  
72 they are implemented using the weak formulation, wherein a set of background  
73 cells are used for integrating the weak form. The so-called conformability of inte-  
74 gration cells vis-à-vis the distribution of particles and supports of shape functions  
75 determine the accuracy of integration and convergence of solutions thereof. How-  
76 ever, the MLPG method eminently bypasses the non-conformability issue (Atluri  
77 and Zhu 1998, Atluri *et al.* 1999, Atluri *et al.* 2000, Atluri and Zhu 2000). Yet an-  
78 other limitation of most mesh-free methods is the sensitive dependence of solutions  
79 on the supports of window functions. The size of the support is only constrained  
80 by the minimum number of particles that it must contain to ensure the invertibility  
81 of the moment matrix (Han and Meng 2001). While a not-too-small support size  
82 prevents the moment matrix from being singular, a very large size might lead to  
83 excessive smoothness of the approximation. In the absence of a strictly quantita-  
84 tive criterion to arrive at the optimal support size, one typically resorts to costly  
85 numerical experiments to choose the right size. Moreover, most mesh-free shape  
86 functions are non-interpolating and hence may not strictly qualify as test functions  
87 as they do not vanish over the essential part of the domain boundary.

88 While mixed FE methods, which are capable of obtaining smooth stress or strain  
89 fields, have been extensively researched, they involve a significant augmentation  
90 of the degrees-of-freedom (DOF-s). Moreover, each mixed method with both dis-  
91 placements and their derivatives as DOF-s has to grapple with certain stability is-  
92 sues (Zienkiewicz, *et al.* 1967). Stabilization techniques are extensively reported  
93 in the literature (Hughes 1995; Hughes *et al.* 2004; Onate *et al.* 2006). Despite  
94 considerable research in developing and understanding the stability of mixed meth-  
95 ods, the (unconditional or parameter-independent) coercivity of the bilinear form  
96 (especially following linearizations of nonlinear PDE-s) is not guaranteed (see, for  
97 instance, Auricchio *et al.* 2005) and may be extremely sensitive to element aspect  
98 ratios (Ainsworth and Coggins 2000). In fact, for linear systems, an analysis of  
99 the bilinear form often yields parameter bounds that are not sharp and this is yet  
100 another source of difficulty. In these techniques, accordingly, the parameters in the  
101 stabilizing terms in the weak form are generally arrived at through rigorous numeri-  
102 cal experiments. Attempts have been made at developing mixed mesh-free methods  
103 that promise improved numerical behaviour against locking (for instance, the mixed  
104 MLPG method; Atluri *et al.* 2004, 2006a, 2006b; Soric and Jarak 2010). Since they  
105 admit an increased number of unknowns (displacements and strains and/or stresses)  
106 in the formulation, they can also handle the singularity issues which might arise due  
107 to ill-behaved derivatives of MLS shape functions. In particular, the mixed finite

108 volume MLPG method (Atluri *et al.* 2004) interpolates displacements and strains;  
109 uses Heaviside's step function as the test function and hence bypass domain inte-  
110 gration. The reduced support size speeds up the computation, thus compensating  
111 for the increased number of unknowns. However, to the authors' knowledge, no  
112 attempts on obtaining the sharp bounds on the coercivity constant have so far been  
113 made. Other methods to arrive at such smooth solutions include Trefftz methods,  
114 the boundary integral method, and the discontinuous Galerkin methods. The Tre-  
115 fftz method (Gamallo and Astley 2007) share some similarities with the boundary  
116 element as well as penalty methods and thus requires a known solution to the ho-  
117 mogeneous problem, which may not always be available for linear systems and/or  
118 locally linearized forms of many (possibly most) nonlinear systems. Here, as in the  
119 discontinuous Galerkin method (Engel *et al.* 2002), the higher order (typically  $C^1$ )  
120 continuity is only weakly enforced by penalizing the jump in the first order normal  
121 derivative across the inter-element boundary. Unfortunately, enforcing  $C^2$  or still  
122 higher order global continuity in this way could be quite formidable. Moreover,  
123 boundary integral techniques (like the boundary element and Trefftz methods; Kita  
124 and Kamiya 1995), whilst bypassing domain integration, result in thickly populated  
125 stiffness matrices that demand special solvers and typically yield spurious solutions  
126 near the domain boundary.

127 The NURBS-based parametric method (Shaw and Roy 2008a) provides smooth so-  
128 lutions for the derivatives by combining the FE-based domain discretization with  
129 the global smoothness polynomial reproducing shape functions. Here a (bijec-  
130 tive) geometric map, constructed through NURBS, is defined between the physi-  
131 cal domain and a rectangular (cuboidal) parametric domain. The shape functions  
132 and their derivatives are obtained over the parametric domain (with trial functions  
133 constructed through tensor-product NURBS) so that polynomial reproduction and  
134 interpolation properties get satisfied over the physical domain. The selection of  
135 support size here is automatic and the integration cells are the NURBS cells them-  
136 selves. But for most practical cases (e.g. for non-simply connected domains), a ge-  
137 ometric map may not exist. To overcome this limitation, Shaw *et al.* (2008b) have  
138 proposed a NURBS-based parametric bridging method, wherein the physical do-  
139 main is decomposed into a finite number of sub-domains such that a geometric map  
140 can be established for each of them. NURBS-based basis functions, constructed  
141 over each sub-domain, are appropriately blended across these sub-domains.

142 Use of the geometric map in the parametric methods above could cause ill-condition-  
143 ing of the discretized equations and numerical pollution. Moreover, owing to the  
144 dual use of knots as particles, the integration of the weak form is not necessarily  
145 conformal. Since discretization of complex domains (say, in 2D) is best handled via  
146 triangulation and a scheme based on globally smooth shape functions constructed

147 using such triangles would work without a geometric map, we presently address the  
 148 question on whether such a scheme can be worked out via triangular B-splines or  
 149 triangular NURBS replacing the tensor-product NURBS in the parametric method.  
 150 Specifically, we employ DMS splines (DMS being an acronym for Dahmen, Mic-  
 151 chelli and Seidel, authors who introduced the spline; Dahmen *et al.* 1992) as the  
 152 window (kernel) functions. The DMS-splines are defined as weighted sums of  
 153 simplex splines over triangles. A key element of this construction is the knotclouds  
 154 that help achieve  $C^{n-1}$  continuity of  $n$ th degree DMS-splines across inter-triangular  
 155 boundaries. Presently, the physical domain in  $\mathbb{R}^2$  is discretized into triangles using  
 156 Delaunay triangulation. This provides this scheme a ready interface with the FEM  
 157 wherein a similar discretization is often made use of. Unlike the FEM, however,  
 158 the shape functions, derived based on the condition of reproduction of polynomials,  
 159 possess inter-element continuity higher than  $C^0$ . Here the particles are located at  
 160 the vertices as well as on the sides and interior of a triangle. The number of parti-  
 161 cles depends on the degree of DMS-splines. Depending on the choice of knots, the  
 162 smooth shape functions, so derived, are supported within a close neighbourhood  
 163 of the corresponding triangle. A procedure to generate the knotclouds whilst en-  
 164 suring non-singularity is also outlined. Integration for the weak form equations is  
 165 done over each triangle so that there is no misalignment of integration cells with  
 166 the arrangement of nodes or the support of the globally smooth shape functions.  
 167 The paper is organised as follows. In Section 2, following a brief account of De-  
 168 launay triangulation, we provide the details of the construction of DMS-splines,  
 169 generation of knotclouds and the evaluation procedure for such splines. In Sec-  
 170 tion 3, a procedure for obtaining the globally smooth shape functions and their  
 171 derivatives with DMS-splines as kernel functions is described. Numerical results  
 172 of example problems are discussed in Section 4 followed by concluding remarks in  
 173 Section 5.

## 174 **2 DMS-Splines and Their Evaluation Schemes**

175 Evaluation routines of DMS-splines have been developed by Fong and Seidel (1992),  
 176 Pfeifle (1994) and Franssen (1995). The last author explains the evaluation scheme  
 177 for  $s$ -variate DMS-splines of degree  $n$ . An essential element for constructing DMS-  
 178 splines is a triangulation of the domain. In particular, we employ Delaunay triangu-  
 179 lation  $D_T(\mathbf{X})$ , which is a triangulation for a set  $\mathbf{X}$  of points in a plane such that no  
 180 point in  $\mathbf{X}$  is inside the circumcircle of any triangle in  $D_T(\mathbf{X})$ . Delaunay triangu-  
 181 lation maximizes the minimum of all the angles of the triangles in the triangulation.  
 182 By definition, the circumcircle of a triangle formed by three points from the origi-  
 183 nal point set is empty if it does not contain vertices other than the three that define  
 184 it. The Delaunay condition states that a triangle net is a Delaunay triangulation if

185 the circumcircles of all the triangles in the net are empty. This definition can be  
 186 extended to 3-D domains by using a circumscribed sphere in place of the circum-  
 circle.

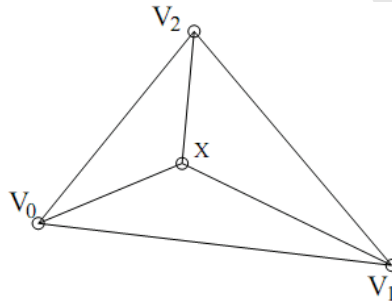


Figure 1: Illustration of barycentric co-ordinates of  $x$  with respect to a triangle  $v_0, v_1, v_2$ ; they are the ratios between the areas of the separate sub-triangles to the area of the entire triangle

187

188 DMS-splines (also called as triangular B-spline), developed by Dahmen, Micchelli  
 189 and Seidel (1992), are essentially weighted sums of simplex splines. They combine  
 190 the overall global smoothness of simplex splines with the local control properties  
 191 of B-patches (Franssen 1995). For completeness and a ready reference, DMS-  
 192 splines in 2-D are briefly touched upon. Also outlined are the method of generating  
 193 knotclouds and evaluation procedures of simplex and DMS-splines.

The  $j^{th}$  barycentric co-ordinate of a point  $x$  in  $\mathbb{R}^2$ , with respect to a triangle with vertices,  $v_0, v_1$  and  $v_2$  for  $0 \leq j \leq 2$  is given by:

$$\lambda_j(\mathbf{x}|v_0v_1v_2) = \frac{Vol((v_0v_1v_2)(v_j:=x))}{Vol(v_0v_1v_2)} \quad (1a)$$

Thus one may write

$$\mathbf{x} = \int_{j=0}^2 \lambda_j(\mathbf{x}|v_0v_1v_2) v_j \quad (1b)$$

194 The half-open convex hull of a triangle  $V$ , denoted as  $[V)$ , is a subset of the convex  
 195 hull of a triangle, such that for every point  $x$  in a triangulation one can determine  
 196 exactly one triangle to which  $x$  belongs. Thus, for  $x$  lying on an edge shared by two  
 197 triangles, it still only belongs to only one of the half-open convex hulls of those  
 198 triangles. But, if  $x$  lies on the boundary of the discretized domain, it might not

199 belong to any triangle, although it does belong to the convex hull of the polygon.  
 200 An exposition on how to arrive at the half-open convex hull of a triangle is available  
 201 in Franssen (1995).

## 202 2.1 Simplex Splines

203 The simplex spline is a multivariate generalization of the well-known univariate  
 204 B-splines. A degree  $n$  simplex spline is a smooth, degree  $n$  piecewise polynomial  
 205 function defined over a set of  $n + N_{dim} + 1$  points  $\mathbf{x} \in \mathbb{R}^{N_{dim}}$  called knots and the set  
 206 of knots, knotset. If the knotset does not contain a collinear subset of (3 or more)  
 207 knots then the simplex spline has overall  $C^{n-1}$  continuity. A detailed discussion of  
 208 the theory of simplex splines is available in Micchelli (1995). We presently focus  
 209 on bivariate simplex splines. A simplex spline defined over a knotset  $V$  is denoted  
 210 as  $M(\cdot|V)$  and its value at  $\mathbf{x} \in \mathbb{R}^2$  is denoted as  $M(\mathbf{x}|V)$ .

A constant simplex spline, defined over 3 knots and knotset  $V = \{v_0, v_1, v_2\}$ , is given by:

$$M(\mathbf{x}|V) = \begin{cases} \frac{1}{|\det(V)|} & \text{if } \mathbf{x} \in [V] \\ 0 & \text{if } \mathbf{x} \notin [V] \end{cases} \quad (2)$$

A higher order simplex spline of degree  $n$  with knotset  $V$  is defined recursively as a weighted sum of three simplex splines, each of degree  $n - 1$ . The number of vertices of the polygon over which  $n$ th degree simplex spline is defined is  $m = n + 2 + 1$ . So the cardinality of  $V$  is  $n + 3$ . The knotsets for the three  $n - 1$  degree simplex splines are chosen from  $V$ , leaving out one of the selected knots from  $V$  at a time as shown in Fig.2 in which the construction of a quadratic simplex spline is explained. The selected knots are marked by double circles. The support of the simplex spline is the half-open convex hull of  $V$ . The quadratic simplex spline is a weighted sum of three linear simplex splines, the domains of which are shown in Fig.2. Barycentric co-ordinates of  $\mathbf{x}$  with respect to the selected triangle formed by the circled knots are used as the weights for the degree  $n - 1$  simplex splines when evaluated at  $\mathbf{x}$ . The recursive formula for the evaluation of degree  $n$  simplex splines is thus given by:

$$M(\mathbf{x}|V) = \int_{j=0}^2 \lambda_j(\mathbf{x}|W) M(\mathbf{x}|V \setminus \{w_j\}) \quad (3)$$

211 where  $W = \{w_0, w_1, w_2\} \subset V$  is the selected (non-degenerate) triangle. Any such  
 212  $W$  from the knotset  $V$  is sufficient to generate the simplex spline of degree  $n$  at  
 213  $\mathbf{x}$ . While the constant simplex spline is discontinuous at its domain boundary, the  
 214 linear simplex spline is  $C^0$  and the degree- $n$  simplex spline is  $C^{n-1}$  everywhere  
 215 (Franssen 1995).

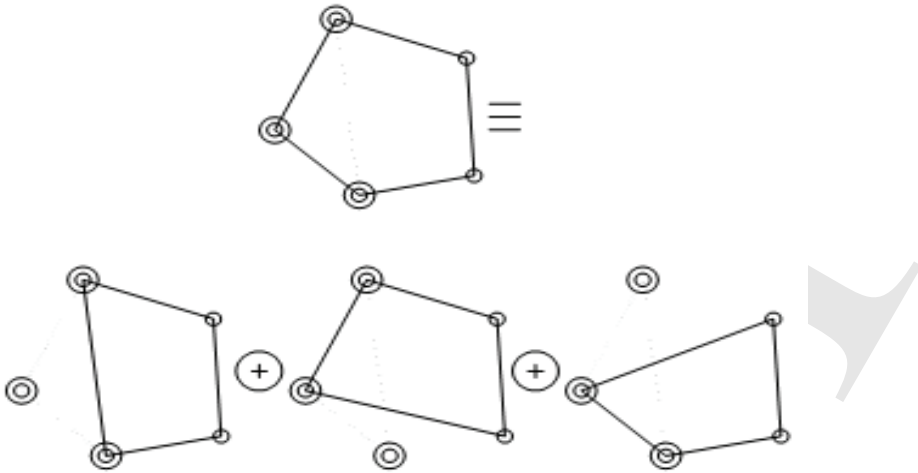


Figure 2: Selection of knotsets for 3 linear simplex splines to generate a quadratic simplex spline as their weighted sum: out of the three knots selected, one is left out, respectively, to form knotsets for the linear simplex splines

216 **2.2 DMS-splines in  $\mathbb{R}^2$**

217 DMS-splines, which are weighted sum of simplex splines, are functions that com-  
 218 bine the global smoothness of simplex splines with the desirable local control fea-  
 219 ture of B-patches (see Franssen 1995 for a detailed exposition). The domain of a  
 220 DMS-spline surface is a proper triangulation  $\mathcal{S} \subset \mathbb{R}^2$ . In every vertex  $v_i$ , a knot-  
 221 cloud of  $n + 1$  knots, denoted as  $\{v_{i0}, \dots, v_{in}\}$  with  $v_{i0} = v_i$ , is defined. The knotsets  
 222 are defined from these knotclouds. A set of control points in  $\mathbb{R}^3$  are defined for each  
 223 triangle  $I \in \mathcal{S}$  for a degree  $n$  surface. The control points are denoted as  $c_\beta^I$  where  
 224  $\beta$  is a triple  $(\beta_0, \beta_1, \beta_2)$  with  $|\beta| = \beta_0 + \beta_1 + \beta_2 = n$ . There are exactly  $\frac{(n+1)(n+2)}{2}$   
 225 such  $\beta$ . The projections of the control points from  $\mathbb{R}^3$  to  $\mathbb{R}^2$  serve as particles in the  
 226 generation of shape functions. A triangular domain, knotclouds and projection of  
 227 control points on  $\mathbb{R}^2$  ( $c_\beta^I$ ) for constructing a quadratic DMS-spline in 2D is shown  
 228 in Fig.3. The closer  $c_\beta^I$  lies to a vertex  $v_j$  of  $I$ , the more knots are taken from the  
 229 corresponding knotcloud to form the knotset in the construction of simplex splines.

Let  $\check{V}_\beta^I = \{v_{0\beta_0}^I, v_{1\beta_1}^I, v_{2\beta_2}^I\}$  be a triangle consisting of the last knots of the heads  
 of knotclouds in  $V_\beta^I$ . The constant multiplier of  $M(\cdot | V_\beta^I)$  in the calculation of a  
 DMS-spline is  $|\det(\check{V}_\beta^I)|$ . The DMS-spline basis functions at  $\mathbf{x}$  corresponding to

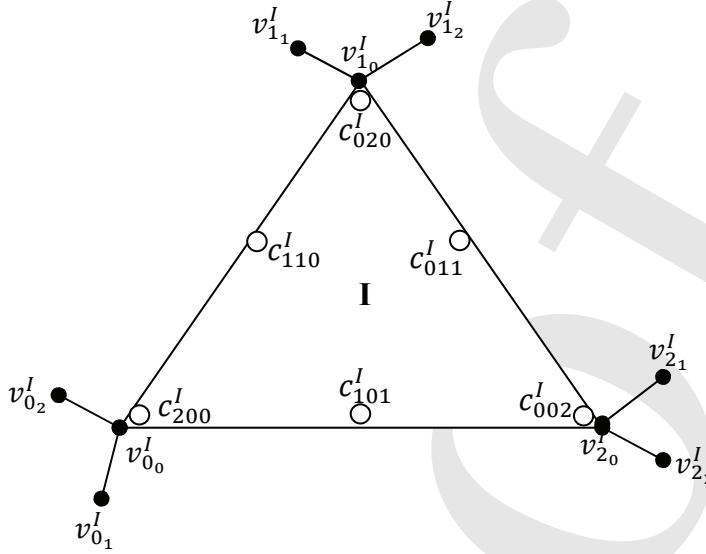


Figure 3: Parameters for a quadratic DMS-spline: the knotclouds of all vertices are the set  $V_{\beta}^I = v(0_0)^I, v(0_1)^I, v(0_2)^I, v(1_0)^I, v(1_1)^I, v(1_2)^I, v(2_0)^I, v(2_1)^I, v(2_2)^I$  and  $c_{\beta}^I$  are control points; the black circles represent knots and white circles, control points

$c_{\beta}^I$  is  $\left| \det \left( \check{V}_{\beta}^I \right) \right| M \left( \mathbf{x} | V_{\beta}^I \right)$ . The point on a surface corresponding to  $\mathbf{x} \in \mathbb{R}^2$  is given by

$$F(\mathbf{x}) = \int_{I \in \mathcal{I}} \int_{|\beta|=n} \left| \det \left( \check{V}_{\beta}^I \right) \right| M \left( \mathbf{x} | V_{\beta}^I \right) c_{\beta}^I \quad (4)$$

230 It is proved (Dahmen *et al.* 1992) that  $\left| \det \left( \check{V}_{\beta}^I \right) \right| M \left( \mathbf{x} | V_{\beta}^I \right) \geq 0 \quad \forall I \in \mathcal{I}$  and  
 231  $\beta, |\beta| = n$  and  $\int_{I \in \mathcal{I}} \int_{|\beta|=n} \left| \det \left( \check{V}_{\beta}^I \right) \right| M \left( \mathbf{x} | V_{\beta}^I \right) = 1$  (partition of unity). A triangle  
 232  $I \in \mathcal{I}$  may also have non-zero contributions to points  $\mathbf{x}$  in the domain that do not  
 233 belong to the half-open convex hull of the triangle. This is a fundamental difference  
 234 with the usual Bézier patch surface, whose values can be evaluated for each patch  
 235 independently. This interference of triangles amongst themselves establishes the  
 236 overall global smoothness of DMS-splines. The part of the surface corresponding  
 237 to a specific triangle  $I$  is a DMS-patch, which is not only the contribution of this  
 238 triangle, but the sum of contributions of all triangles to the point  $\mathbf{x} \in I$ .

### 239 2.3 Generation of Knotclouds

240 The knotclouds serve as a universal set for a triangle from which knotsets for sim-  
 241 plex splines in the calculation of DMS-splines are derived. A major restriction  
 242 on the placement of knotclouds is that no three knots in it can be collinear. This  
 243 warrants extreme care to be exercised whilst generating the knotclouds over the  
 244 (bounded) physical domain. In addition to collinearity, two additional restrictions  
 245 are imposed to guarantee affine invariance (Franssen 1995):

- 246 1. If  $\Omega'$  is the interior of  $\bigcap_{|\beta| \leq n} [\check{V}'_{\beta}]$ , then  $\Omega' \neq \emptyset$ , where  $\emptyset$  is a subset with  
 247 zero area.
- 248 2. In a triangle  $I = \{v_p, v_q, v_r\}$ , if one of the edges, say  $(v_p, v_q)$ , is on the bound-  
 249 ary, then the knotclouds for  $v_p$  and  $v_q$  must be placed on the opposite side of  
 250 the boundary edge  $(v_p, v_q)$  with respect to that for  $v_r$ .

251 The first of the above is necessary for all DMS-splines. But the second one is im-  
 252 portant for surface reconstructions that do not include the whole of  $\mathbb{R}^2$ . Following  
 253 this restriction, the knotclouds on the boundary of a domain may preferably be  
 254 placed outside the domain. This will help avoid collinearity of knots and awkward  
 255 polygonal shapes.

256 For the construction of degree  $n$  DMS-splines,  $n$  knots need to be added at each  
 257 vertex of all the triangles in the triangulation. The following procedure is adopted  
 258 for adding and placing knots at each vertex of a triangle:

- 259 • From the triangulation data available with Delaunay procedure, the boundary  
 260 vertices of the physical problem domain are separated.
- 261 • For a vertex  $v_i$ , all the triangles which share it are located.
- 262 • The included angles  $(\theta_{int}^j, j = 1, 2, \dots, m)$  made by the triangles at  $v_i$  are  
 263 calculated. Here  $\theta_{int}^j$  is the  $j^{th}$  included angle for an internal vertex  $v_i$  (one  
 264 that belongs to the domain interior) and  $m$  is the number of included angles  
 265 (equal to number of triangles sharing  $v_i$ ). The exterior angle ( $\theta_{ext}$ ) subtended  
 266 by the boundary edges at the vertex  $v_i$ , when the latter is on the boundary, is  
 267 also calculated.
- 268 • For an internal vertex  $v_i$ , elements of  $\{\theta_{int}^j\}$  are sorted in the descending order  
 269 of their magnitudes. The knot placement is done along lines originating from  
 270  $v_i$  and along directions obtained by dividing the angles as follows. If  $m \geq n$ ,  
 271  $\theta_{int}^j, j = 1, 2, \dots, n$  are bisected to get the lines. If  $m < n$  and  $n = km + r$ ,

272 where  $r$  is the remainder of  $n/m$ ,  $\theta_{int}^j$ ,  $j = 1, 2, \dots, r$  will be divided equally  
273  $(k + 1)$  times and the rest  $(m - r)$  angles,  $k$  times so that  $n$  lines are created.

274 • The distance of a knot from a vertex  $v_i$ , called knot-length, is chosen opti-  
275 mally (in some sense) based on the following observation. If it is too large  
276 or small, the knots of adjacent vertices may move either closer towards each  
277 other or to  $v_i$ , which may lead to irregular distribution of knots for the con-  
278 struction of simplex splines. The knot-length is arrived at as follows: The  
279 lengths of all edges of triangles meeting at  $v_i$  are calculated and the smallest  
280 among them is selected. Roughly 5 to 10% of this length is chosen as the  
281 knot-length for all knots to be placed near that vertex. This choice is found  
282 to work well for many problems, as numerically demonstrated later.

283 • A line is assumed along each division of the angle and a knot is placed on  
284 this line at the chosen knot-length from the associated  $v_i$ .

285 • For a boundary vertex  $v_i$ , the same procedure as that for the interior vertices  
286 is followed. The knots are then reflected (rotated by 180) to the exterior of  
287 the domain.

288 The knotcloud generation for a bracket, which has internal and external boundaries,  
289 are shown in Fig.4(a) and (b) en route the construction of quadratic and cubic DMS-  
290 splines.

## 291 2.4 Recursive Evaluations of Simplex and DMS-splines in 2D

292 Simplex splines of degree  $n$  are weighted sums of three simplex splines of degree  
293  $n - 1$ . DMS-splines of degree  $n$ , on the other hand, are weighted sum of simplex  
294 splines of degree  $n$ .

### 295 2.4.1 Evaluation of simplex splines

296 As noted before (Eq. 2), a constant simplex spline, over a triangle  $V$  with ver-  
297 tices (knotset)  $V = \{v_0, v_1, v_2\}$ , is evaluated as  $M(\mathbf{x}|V) = \begin{cases} \frac{1}{|det(V)|} & \text{if } \mathbf{x} \in [V] \\ 0 & \text{if } \mathbf{x} \notin [V] \end{cases}$ .

298 For the determinant  $|det(V)|$  to be non-zero,  $\mathbf{x}$  should lie in the half-open con-  
299 vex hull of  $V$  ( $[V]$ ). The domain over which a linear simplex spline is defined in  
300  $\mathbb{R}^2$  is a quadrilateral (i.e., the polygon connecting the four knots is the quadrilat-  
301 eral). Let  $V = \{v_0, v_1, v_2, v_3\}$  be the knotset for a linear simplex spline. A degree  
302  $n$  simplex spline is evaluated over an  $(n + 3)$ -sided polygon as the weighted sum  
303 of three  $(n - 1)$  degree simplex splines. The knotset  $V$  contains  $(n + 3)$  knots, i.e.

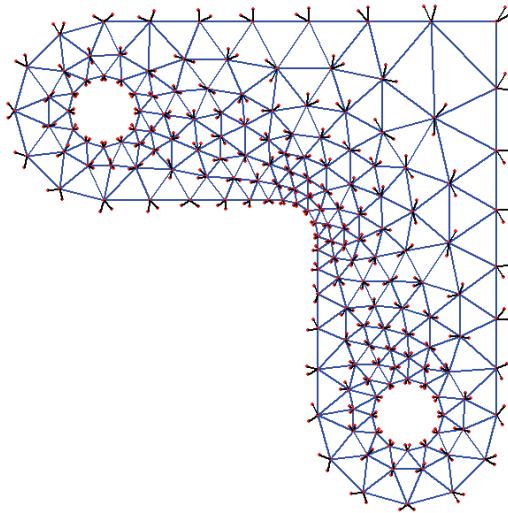


Fig 4(a)

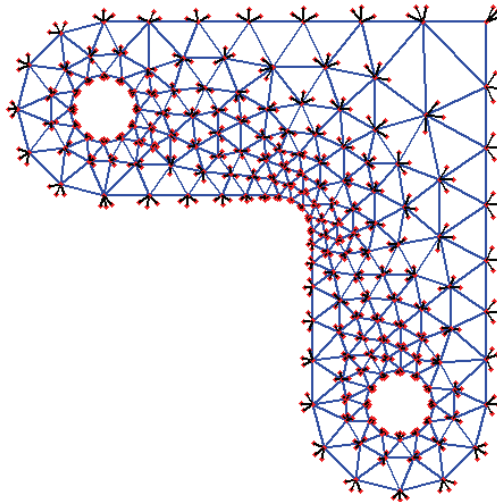


Fig 4(b)

Figure 4: Knot generation in a bracket after triangulation to construct (a) quadratic DMS-splines and (b) cubic DMS-splines

304  $V = \{v_0, v_1, \dots, v_{n+1}, v_{n+2}\}$ . The recurrence formula is given as Eq. (3). The for-  
 305 mula involves the evaluation of  $3^{n-1}$  linear simplex splines and  $3^n$  constant sim-  
 306 plex splines in a naïve approach, as shown in Fig.5. But, by carefully identifying  
 307 the repetitions of simplex splines of various degree, number of evaluations can be  
 308 significantly reduced. The first three knots of knotsets of every simplex spline are  
 309 chosen as the set  $W$  (see Eq.3) in a straightforward approach. The number of in-  
 310 dependent linear and constant simplex splines to be evaluated will be  $\frac{n(n+1)}{2}$  and  
 $\frac{(n+1)(n+2)}{2}$ , respectively (Table 1).

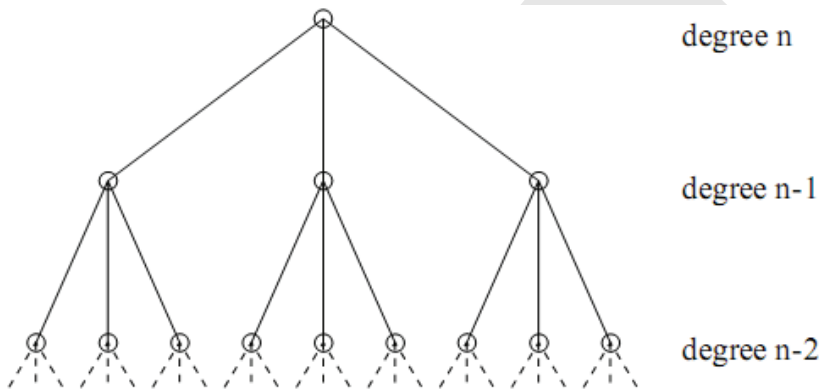


Figure 5: Each node in the tree represents a simplex spline to be evaluated to get the simplex spline represented by the root node; the number of simplex splines in each level =  $k^n$ , where  $k$  is the level of evaluation, starting from top

311

### 312 2.4.2 Evaluation of DMS-splines

313 A degree  $n$  DMS-spline basis function, evaluated at a point  $\mathbf{x} \in \mathbb{R}^2$ , is defined  
 314 over the control points  $c_\beta^I$  (Eq. 4) and is given by  $|\det(\check{V}_\beta^I)| M(\mathbf{x}|V_\beta^I)$ , where  
 315  $M(\mathbf{x}|V_\beta^I)$  is a simplex splines of degree  $n$  and  $\check{V}_\beta^I$ , a triangle consisting of the  
 316 end knots of the knotclouds of the three vertices of the triangle  $I$ , corresponding  
 317 to a control point  $c_\beta^I$ , i.e.  $\check{V}_\beta^I = \{v_{0_{\beta_0}}^I, v_{1_{\beta_1}}^I, v_{2_{\beta_2}}^I\}$ . The number of control points is  
 318 equal to  $\frac{(n+1)(n+2)}{2}$  in  $\mathbb{R}^2$ . For each triangle  $I$  in  $\mathcal{S}$ , the particles are located as the  
 319 projections of control points on the triangle, as shown in Figs.6(a) through (d).

Table 1: Number of evaluations of simplex splines required at each level

Level of evaluation ( $k$ )	Degree of simplex spline	No of evaluations in a naïve scheme	No of independent evaluations done
1	$n$	1	1
2	$n - 1$	3	3
3	$n - 2$	9	6
...	...	...	...
$k$	$n - k + 1$	$3^{k-1}$	$k(k + 1) / 2$
...	...	...	...
$n$	1	$3^{n-1}$	$n(n + 1) / 2$
$n + 1$	0	$3^n$	$(n + 1)(n + 2) / 2$

### 3 Shape Functions and their Derivatives

321 Generation of globally smooth shape functions in 2D domain with DMS-splines  
 322 as weight functions will be discussed in this section. The DMS-spline in  $\mathbb{R}^2$  is  
 323 denoted as  $\Phi(x, y)$ . A DMS-spline is supported over a triangle and its knotcloud  
 324 neighbourhood defined as the polygon formed by connecting the knots, distributed  
 325 following the restrictions mentioned in Section 2.3 and located close to the vertices  
 326 of the triangle. DMS-spline is constructed corresponding to a given nodal point  $\mathbf{x}$  in  
 327 a physical domain in  $\mathbb{R}^2$ , over the triangle to the half-open convex hull of which  $\mathbf{x}$   
 328 belongs. In general, DMS-splines satisfy the partition of unity and their derivatives  
 329 (including the splines themselves) are globally smooth. But, a direct functional ap-  
 330 proximation based on these functions and their derivatives may sensitively depend  
 331 on the placement of knots around the vertices of triangles. Thus, when the knots are  
 332 far away from or very close to the vertices, the DMS-splines may numerically devi-  
 333 ate from the partition of unity property and the total volume under their derivatives  
 334 may not be close to zero, especially for  $\mathbf{x}$  close to or on the boundary of the trian-  
 335 gle. So, use of DMS-splines and their derivatives directly as shape functions and  
 336 derivatives of shape functions (respectively) may lead to considerable errors in the  
 337 approximation of a variable (results from a numerical example to illustrate this is  
 338 given in Figs.11 and 12). We propose to study if an explicit reproduction of polyno-  
 339 mials could help overcome this difficulty. Thus the shape functions are constructed  
 340 by the reproduction of all the elements in a complete set of polynomials (a set con-  
 341 taining all the terms in the Pascal's triangle) of degree  $p \leq n$ , with DMS-splines  
 342 as weight functions. It is hoped that a numerical robust imposition of the partition  
 343 of unity property and global smoothness for the shape functions might be possi-

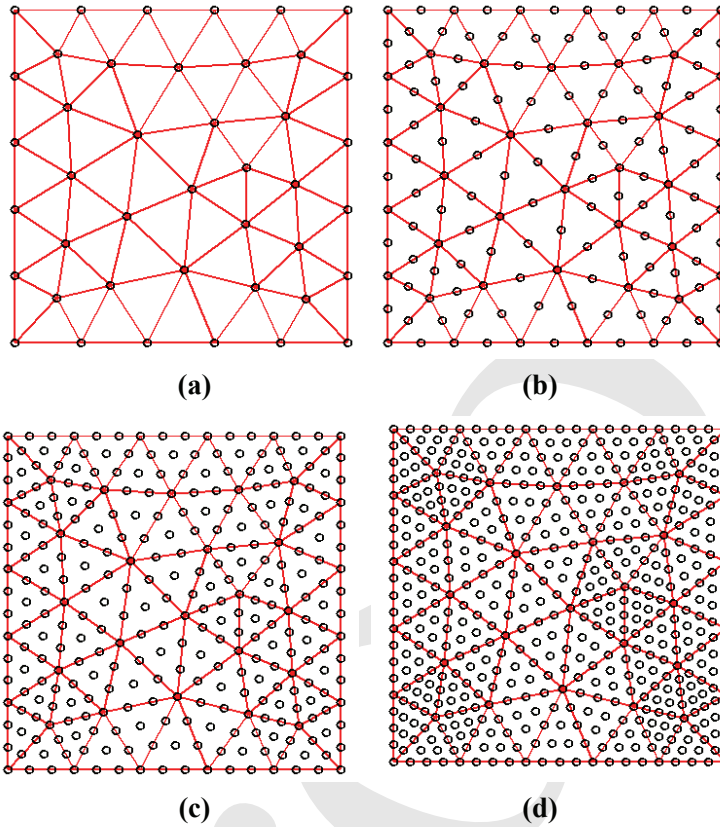


Figure 6: Distribution of particles (projections of control points) for DMS-splines of various degrees ( $n$ ) in a triangulation; the black circles represent particles; (a)  $n=1$ , three particles in a triangle, (b)  $n=2$ , six particles in a triangle, (c)  $n=3$ , ten particles in a triangle, (d)  $n=4$ , fifteen particles in a triangle

344 ble through this route. Accordingly, we also propose to construct the derivatives  
 345 of shape functions by reproducing the corresponding derivatives of elements of a  
 346 complete polynomial set with DMS-splines as weight functions, following Shaw  
 347 and Roy (2008a).

### 348 3.1 Generation of Shape Functions

Consider a bounded domain  $\Omega \subset \mathbb{R}^2$  and a sufficiently smooth function  $u(x, y)$ , which is required to be approximated over the domain. Consistent with the FEM or a mesh-free method, an approximant  $u^a(x, y)$  to the targeted function is assumed

to be of the form:

$$u^a(x, y) = \int_{i=1}^{N_{nd}} \Psi_i(x, y) u_i \quad (5)$$

where  $N_{nd}$  represents the number of nodes in the domain,  $u_i = u(x_i, y_i)$  is the value of the targeted function at particle  $i$  and  $\Psi_i(x, y)$  are the globally smooth shape functions. Following the practice in many mesh-free methods (e.g. the reproducing kernel methods (Liu, *et al.* 1995a, Shaw, *et al.* 2008a, etc), the latter can be written as:

$$\Psi_i(x, y) = \mathbf{H}^T(x - x_i, y - y_i) b(x, y) \Phi(x - x_i, y - y_i) \quad (6)$$

where  $\mathbf{H}^T(x, y)$  is a set of polynomials defined as  $\{x^\alpha y^\beta\}_{|\alpha+\beta|\leq p}$ ,  $p$  is degree of polynomial ( $p \leq n$ ),  $b(x, y)$  are coefficients of the polynomials in  $\mathbf{H}$  and  $\Phi(x - x_i, y - y_i)$  is the DMS-spline based at  $(x_i, y_i)$  acting as the weight function. The coefficients  $b(x, y)$  are obtained based on the following polynomial reproduction conditions:

$$\int_{i=1}^{N_{nd}} \Psi_i(x, y) 1 = 1 \quad (7)$$

$$\int_{i=1}^{N_{nd}} \Psi_i(x, y) (x_i^\alpha y_i^\beta) = x^\alpha y^\beta \quad |\alpha + \beta| \leq p \quad (8)$$

$$\int_{i=1}^{N_{nd}} \Psi_i(x, y) ((x - x_i)^\alpha (y - y_i)^\beta) = \delta_{|\alpha||\beta|,0} \quad |\alpha + \beta| \leq p \quad (9)$$

$$\int_{i=1}^{N_{nd}} \mathbf{H}^T(x - x_i, y - y_i) b(x, y) \Phi(x - x_i, y - y_i) \mathbf{H}(x - x_i, y - y_i) = \mathbf{H}(0)$$

$$\mathbf{M}(x, y) b(x, y) = \mathbf{H}(0)$$

Here

$$\mathbf{M}(x, y) = \int_{i=1}^{N_{nd}} \mathbf{H}^T(x - x_i, y - y_i) \Phi(x - x_i, y - y_i) \mathbf{H}(x - x_i, y - y_i) \quad (10)$$

is the so-called moment matrix. So the coefficient vector is given by:

$$b(x, y) = \mathbf{M}^{-1}(x, y) \mathbf{H}(0)$$

provided that the moment matrix is invertible. We will be considering this issue shortly. Presently, the global shape functions in two-dimensions are given by:

$$\Psi_i(x, y) = \mathbf{H}^T(x - x_i, y - y_i) \mathbf{M}^{-1}(x, y) \mathbf{H}(0) \Phi(x - x_i, y - y_i) \quad (11)$$

349 If a nodal point  $\mathbf{x}$  is inside a triangle, the support of the shape function is defined  
 350 by a polygon that contains the triangle and is formed by the knotcloud associated  
 351 with the vertices of that triangle as shown in Fig. 7a. If  $\mathbf{x}$  falls on an edge shared  
 352 by two triangles, the polygonal support of the shape function will include both the  
 353 triangles sharing that edge as shown in Fig. 7b. As a third alternative, if  $\mathbf{x}$  coincides  
 354 with a common vertex shared by several triangles, then the support for the shape  
 355 function will be in the form of a polygon containing all these triangles which share  
 356 that vertex (Fig. 7c).

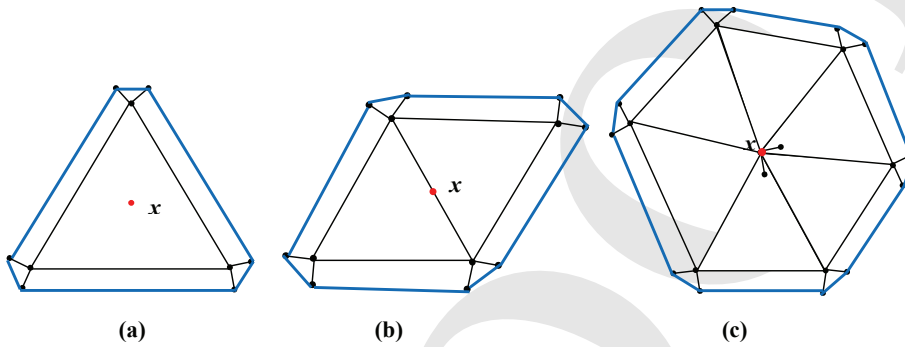


Figure 7: Supports (outer polygons) of shape functions when the nodal point  $\mathbf{x}$  (red dot) is (a) inside a triangle, (b) on an edge shared by two triangles and (c) on one of the vertices of triangles; the knotcloud shown as black dots is for quadratic DMS-splines

### 357 3.2 Derivatives of Shape Functions

A stable and numerically accurate scheme for computing derivatives of globally smooth shape functions has been proposed by Shaw and Roy (2008a). It is based on the premise that  $\gamma^h$  derivatives of such shape functions reproduce  $\gamma^h$  derivatives of any arbitrary element of the space  $P_p$  of polynomials of degree  $p \geq |\gamma|$ . Using this principle, consistency relations for the derivatives may be written as:

$$\int_{i=1}^{N_{nd}} \Psi_i^{(\gamma)}(x, y) \mathbf{H}(x - x_i, y - y_i) = (-1)^{|\gamma|} \mathbf{H}^{(\gamma)}(0), \quad \forall |\gamma| \leq p \quad (12)$$

where  $\Psi_i^{(\gamma)}(x, y) \triangleq D^\gamma \Psi_i(x, y)$  is the  $\gamma$ -th derivative that exactly reproduces  $\gamma^h$  derivatives of elements in the space  $P_p$  for  $p \geq |\gamma|$ . Now,  $\Psi_i^{(\gamma)}(x, y)$  may be written as:

$$\Psi_i^{(\gamma)}(x, y) = H^T(x - x_i, y - y_i) b^\gamma(x, y) \Phi(x - x_i, y - y_i) \quad (13)$$

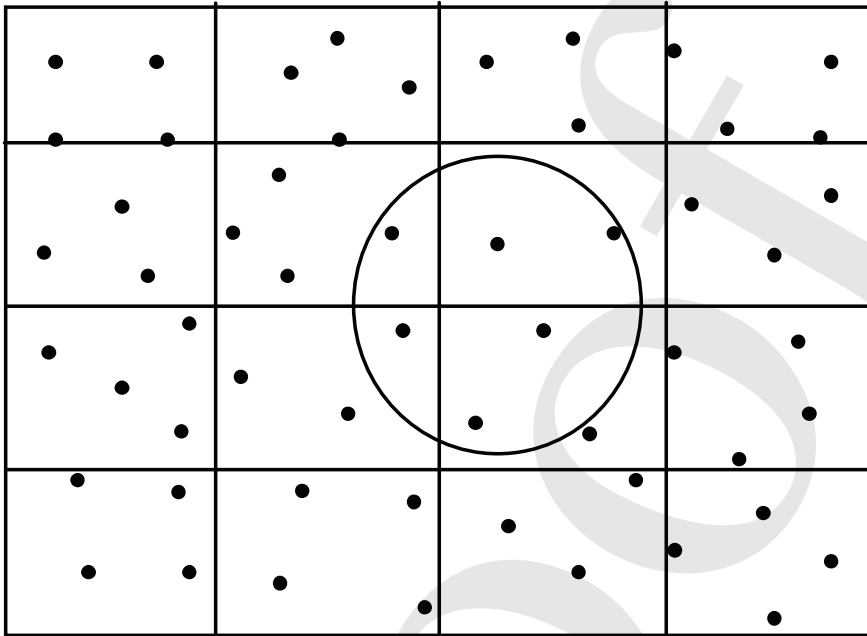


Figure 8: Misalignment of local support domain (circle) and background integration cells (rectangular) in a mesh-free method (particles are black dots)

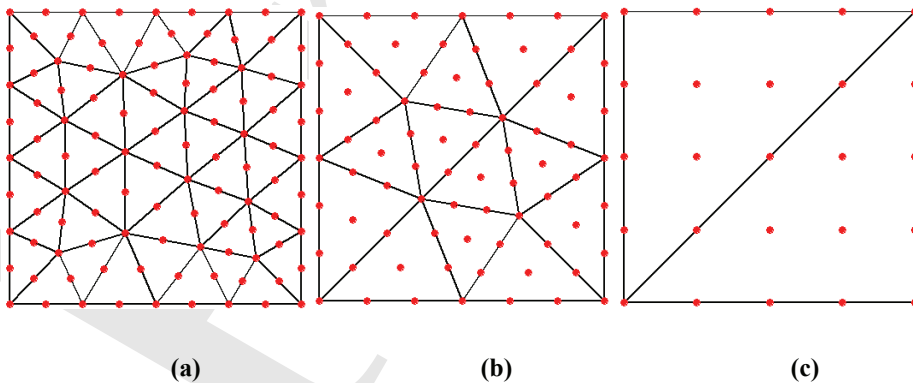


Figure 9: Aligned local domain (triangles) of DMS-spline basis functions and integration cells (triangles) in the present scheme (particles are red dots); fine to coarse triangulations

Here  $b^\gamma(x, y)$  is the vector of unknown coefficients for derivative reproduction. The final form of  $\Psi_i^{(\gamma)}(x, y)$  can be written as:

$$\Psi_i^{(\gamma)}(x, y) = (-1)^{|\gamma|} \mathbf{H}^{(\gamma)}(0) \mathbf{M}^{-1}(x, y) H^T(x - x_i, y - y_i) \Phi(x - x_i, y - y_i) \quad (14)$$

### 3.3 Invertibility of the Moment Matrix

In most of the mesh-free methods, the support of the shape functions (as determined through that of the weight or kernel function) needs to be user-specified subject to such considerations like ensuring invertibility of the moment matrix, adequacy of smoothness of shape functions and limiting computation time. Following Proposition 3.5 in Han and Meng (2001), the necessary condition for the moment matrix  $\mathbf{M}(\mathbf{x})$  at a point  $\mathbf{x} \in \Omega$  to be invertible is that  $\mathbf{x}$  must be covered by at least  $\dim(P_p) = \frac{(p+N_{dim})!}{p!N_{dim}!}$  shape functions, where  $\dim(P_p)$  is the cardinality of the polynomial space of degree  $\leq p$ , and  $N_{dim}$  is the dimension of the domain  $\Omega$ . So, if  $\Omega \subset \mathbb{R}^2$ , the number of shape functions required for ensuring invertibility of  $\mathbf{M}(x, y)$  is  $\frac{(p+2)!}{p!2!} = \frac{(p+2)(p+1)}{2}$ . The number of nodes or particles introduced in a triangle (local support domain of shape functions) is  $\frac{(n+2)(n+1)}{2}$  which will be equal to the number of DMS-spline basis functions corresponding to the control points. The DMS-splines are  $C^{n-1}$  continuous, everywhere, if the knots are in general position (i.e. no three knots are collinear) (Dahmen *et al.* 1992). Therefore, if  $p \leq n$ , the invertibility condition given by Han and Meng will be satisfied, in general. Now, if  $\mathbf{x}$  falls on one of the edges or vertices of a triangle  $I \in \mathcal{I} \subset \mathbb{R}^2$ , it may not always belong to the half open convex hull of all the sub-triangles formed by subsets of the knotsets corresponding to the control points. This may lead to reduction of continuity of DMS-splines by one. In such a case  $n$  has to be kept greater than  $p$  to satisfy the invertibility requirement. In the present method, it is ensured that the minimum number of particles (shape functions) is included in a local support (triangle) to make the moment matrix invertible by choosing  $n = p$  or  $n = p + 1$  as the nodal point  $\mathbf{x}$  is inside or on the boundary of the local support, respectively.

### 3.4 Numerical Integration

In solving the weak form (as in a Galerkin projection) of a system of differential equations, a background mesh (similar to the mesh used in the FEM) is generally required in mesh-free methods for evaluating the integrals that arise. Integration is generally performed over each background cell by a quadrature rule (e.g. Gauss quadrature). Thus a meshing scheme like that in the FEM is anyway required. But, in doing so, the supports of shape functions may not often align (i.e., be identical) with the integration cells (Fig. 8). This may lead to inaccurate integration leading to loss of accuracy and convergence of mesh-free methods (Dolbow and

391 Belytschko 1999). This difficulty is generally overcome via a substantial increase  
 392 in the order of quadrature in many mesh-free methods. In the present scheme, the  
 393 physical domain is initially represented by a triangulation that enables construction  
 394 of the DMS-spline basis functions. Recall from Section 3.1 that the local support  
 395 of the shape functions is a triangle or triangles and associated knotcloud neigh-  
 396 bourhood. But, since the knot lengths (distance to an extra knot associated to a  
 397 vertex from the vertex) are chosen to be very small compared to the triangle edges,  
 398 the local support may be considered as the triangle or triangles themselves for the  
 399 purpose of numerical integration. So, the triangulation itself serves as integration  
 400 mesh in the present scheme. Roughly speaking, a coarse triangulation with higher  
 401 order quadrature or a fine triangulation with lower order quadrature should gener-  
 402 ally give good results. In the NURBS-based parametric bridge method (Shaw, *et al.*  
 403 2008b), since the mesh in the parametric space is used as integration cells, the num-  
 404 ber of such cells will be in excess of what might have been sufficient. Moreover,  
 405 the alignment of integration cells and the supports of shape functions is usually  
 406 not available for  $n > 2$ . In other methods like the element free Galerkin (EFG),  
 407 higher order quadrature is used for more accurate integration. The present scheme  
 408 is free of any such misalignment issues because of the uniformity in the placement  
 409 of knots and the extra knots being not used as particles (nodes). Numerical ex-  
 410 periments with the present method show that just a 3-point Gauss quadrature with  
 411 quadratic DMS-splines (along with a rather fine triangulation; Fig 9a) or a 7-point  
 412 Gauss quadrature with cubic or quartic DMS-splines (with a coarse triangulation;  
 413 Fig 9b and 9c) is adequate to get good accuracy.

### 414 3.5 Imposition of essential boundary conditions

The shape functions in the present scheme, like many other mesh free shape func-  
 tions, do not satisfy the Kronecker delta property. This makes them non-interpolating  
 and hence a direct imposition of Dirichlet boundary conditions is not straightfor-  
 ward. Several solutions to this problem have been reported in the literature (Sonia  
 and Antonio 2004, Cai and Zhu 2004, Shuyao and Atluri 2002, Zhu and Atluri  
 1998, etc.). The penalty method is adopted in this work to impose the Dirichlet  
 (essential) boundary conditions. Thus, consider the boundary value problem given  
 by:

$$\begin{aligned}
 \Delta u &= f & \text{in } \Omega \\
 u &= u_d & \text{on } \Gamma_d, \\
 \nabla u \cdot \mathbf{s} &= g_s & \text{on } \Gamma_s
 \end{aligned}
 \tag{15}$$

where  $\Gamma_d \cup \Gamma_s = \partial\Omega$  and  $\mathbf{s}$  is the outward normal unit vector on  $\partial\Omega$ . If the shape  
 functions are interpolating (so that the test functions are identically zero on the

Dirichlet boundary) the weak form associated with Eq. (15) is:

$$\int_{\Omega} \nabla v \cdot \nabla u d\Omega - \int_{\Gamma_s} v \nabla u \cdot \mathbf{s} d\Gamma = \int_{\Omega} v f d\Omega \quad (16)$$

where  $v$  and  $u$  are the test and trial functions respectively. With the use of the penalizer  $\alpha$ , the weak form can be rewritten as:

$$\int_{\Omega} \nabla v \cdot \nabla u d\Omega - \int_{\Gamma_s} v g_s d\Gamma = \int_{\Omega} v f d\Omega + \int_{\Gamma_d} \alpha (u - u_d) v d\Gamma \quad (17)$$

415 A proper choice of the penalizer  $\alpha$  (usually chosen to be a large positive number)  
 416 should lead to an accurate imposition of the Dirichlet boundary conditions. Indeed,  
 417 as  $\alpha \rightarrow \infty$ , one can show that the solution  $u$  corresponding to the weak form (17) sat-  
 418 isfies the Dirichlet condition. However, quite unlike the NURBS-based parametric  
 419 bridge method (Shaw *et al.* 2008b), shape functions (especially those correspond-  
 420 ing to the triangle vertices) via the present scheme are ‘nearly interpolating’. This  
 421 can be observed from the fact that the typical knot-length is presently smaller than  
 422 the characteristic triangle size by at least an order or more. Hence, referring to Fig.  
 423 7(a) for instance, the triangle and the support of the shape function nearly overlap.  
 424 In other words, using the partition of unity property and the fact that shape func-  
 425 tions must be zero on the support boundary, it follows that the shape function for a  
 426 nodal point nearly attains the value of unity at that node (especially if the node is a  
 427 vertex).

### 428 **3.6 Sparseness of the stiffness matrix**

429 The smoothness in the functional approximation in most meshless methods typi-  
 430 cally require that the ‘band’ of interacting nodes is larger than that in the FEM.  
 431 This leads to a larger bandwidth of the stiffness matrix and in turn an increased  
 432 computational time for the inversion of the discretized equations. While the present  
 433 method shares common FE-based domain decomposition (via Delaunay triangula-  
 434 tion), the shape functions are nevertheless generated by the reproducing kernel par-  
 435 ticle technique. In this context, we recall that the compact support of the proposed  
 436 shape function (as well as its derivatives) is nearly the triangle itself (with respect  
 437 to which it is constructed) and that the compact support contains only the minimum  
 438 number of particles required for the inversion of the moment matrix. This observa-  
 439 tion, combined with the adoption of the triangles themselves as background inte-  
 440 gration cells, naturally leads to the computed system stiffness matrix being sparse  
 441 (i.e., with the smallest bandwidth permissible within the polynomial reproducing  
 442 framework) and hence the sparse equation solvers, often used with commercially  
 443 available FEM codes, can be employed in the present method too.

444 **4 Numerical Results**

445 First, we consider polynomial and non-polynomial (trigonometric and exponential)  
 446 functions, and their derivatives up to fourth order and approximate them over a  
 447 square domain with DMS-spline based global shape functions. The need for poly-  
 448 nomial reproduction in deriving the shape functions is brought forth in the first  
 449 example. Solutions of Laplace's and Poisson's equations and comparisons with ex-  
 450 act solutions are presented next. Solutions of a few second order boundary value  
 451 problems, involving plane stress and plane strain cases, are then attempted with  
 452 the present method and comparisons provided with a few other available methods,  
 453 e.g. the parametric mesh-free method, RKPM and FEM with Q4 (4-noded quadri-  
 454 lateral) as well as T6 (6-noded triangle) elements. Problems involving non-simply  
 455 connected domains are also solved to demonstrate the advantages of the present  
 456 method over the NURBS-based parametric bridge method.  $N_e$  denotes the number  
 457 of triangles in the triangulation, in the following tables and figures.

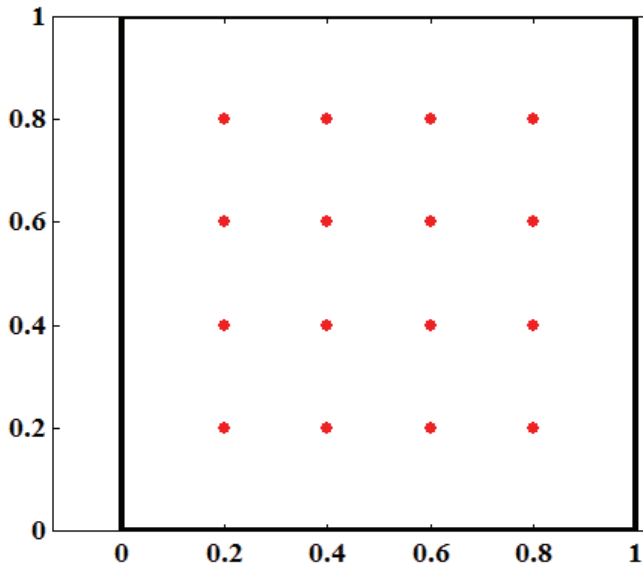


Figure 10: A square domain of dimension  $1 \times 1$ ; the function values and their derivatives are calculated at points marked as red dots

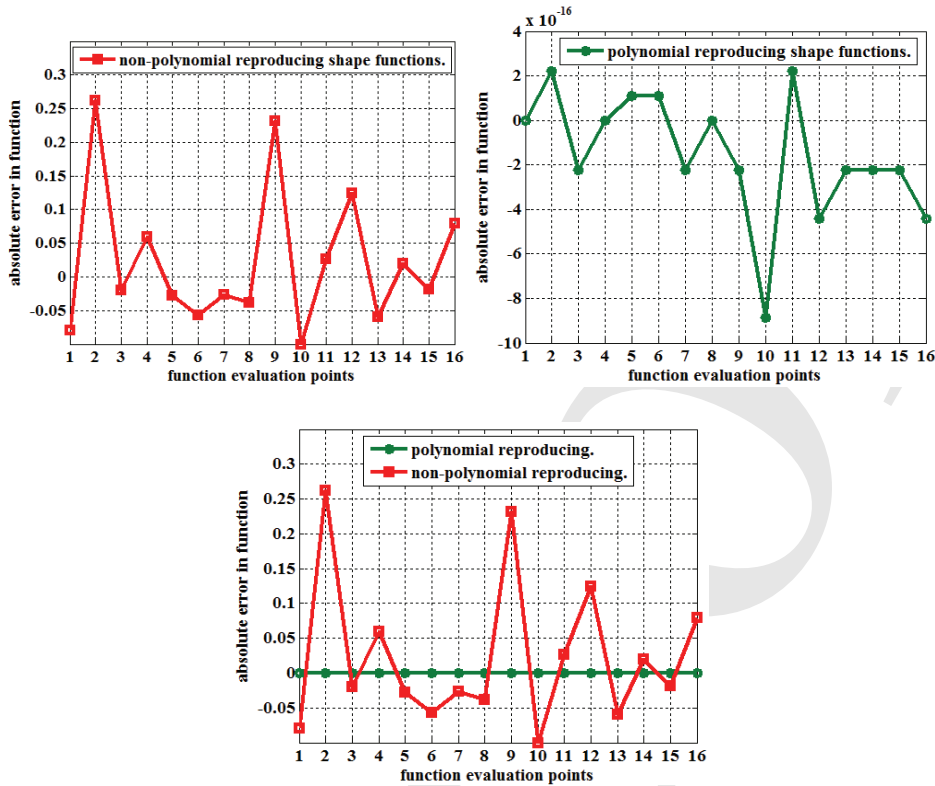


Figure 11: Plots of absolute error magnitudes for  $f(x, y) = x + y$  at the evaluation points; (a) using standard DMS shape functions; (b) using polynomial reproducing DMS shape functions and (c) a direct comparison of errors in both cases

458 **4.1 Approximating a Few Target Functions and their Derivatives**

459 **4.1.1 Polynomial functions**

In order to illustrate the need for polynomial reproduction whilst generating the shape functions, a linear polynomial function,  $f(x, y) = x + y$  and its first derivative with respect to  $x$  are evaluated at 16 points (represented by the red dots in Fig. 10) in a square domain of dimension  $1 \times 1$  (unit<sup>2</sup>) with standard DMS-spline based shape functions (without polynomial reproduction) and polynomial reproducing DMS-spline based shape functions. In both cases, linear DMS-splines are used with the domain being discretized by 16 particles and 18 triangles. The absolute error magnitudes in both cases vis-à-vis the exact values are plotted against the function evaluation points in Figs. 11 and 12. Remarkably, large errors in the approximated

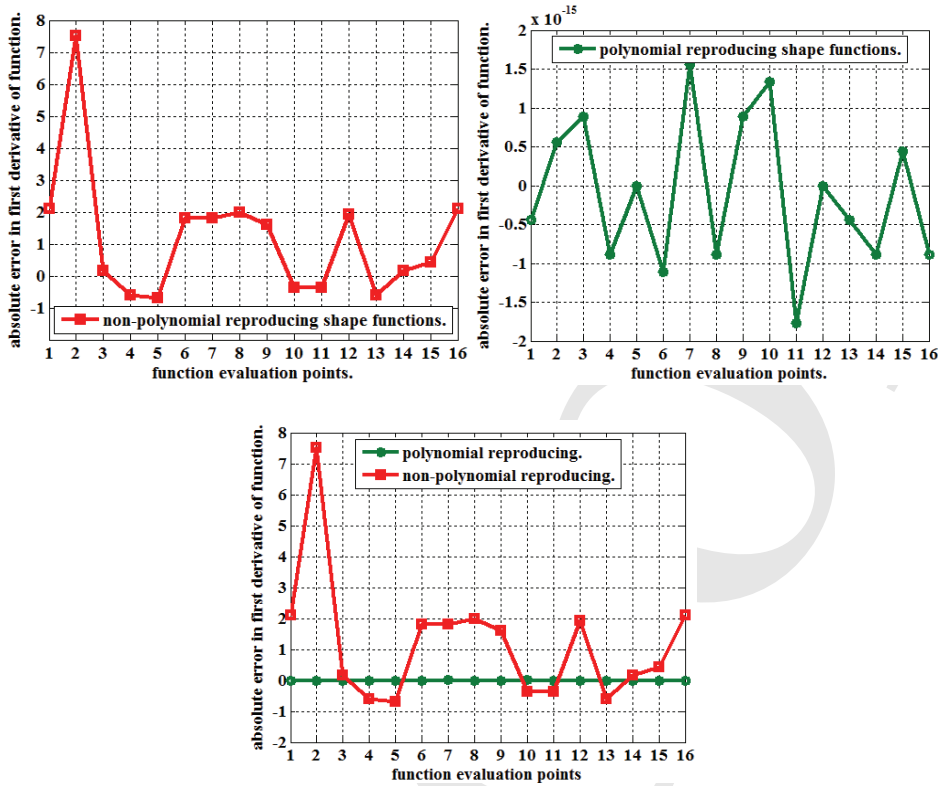


Figure 12: Plot of absolute errors in the first derivative of function  $f(x, y) = x + y$  against the points at which the function is evaluated, (a) using non-polynomial reproducing shape functions (b) using polynomial reproducing shape functions and (c) comparison of errors in both cases

function and its derivative are observed if the explicit condition of polynomial reproduction is dropped in the derivation of the shape functions. Moreover, it is also observed from Table 2 that, while an increase in the degree of DMS-splines does not decrease the error substantially, an increase in the number of triangles reduces the error, to an extent, in the case of standard DMS shape functions. Similar results, shown in Table 3 through the polynomial reproducing shape functions, are once more indicative of the crucial role played by the polynomial reproduction step in obtaining an accurate functional approximation. Indeed, as verified via Table 3, relative  $L^2$  error norms for polynomial functions and their derivatives up to the fourth order via the proposed shape functions are low even when there is only minimum number of triangles (two) in the triangulation of the domain. In these two

tables, the relative  $L^2$  error norm is defined as ( $f^a$  represents the approximant for the targeted function  $f$  over a bounded domain  $\Omega$ ):

$$f - f^a_{L^2} = \frac{\left(\int_{\Omega} (f - f^a)^2 d\Omega\right)^{1/2}}{\left(\int_{\Omega} f^2 d\Omega\right)^{1/2}} \quad (18)$$

460 The construction of the standard DMS-spline basis functions is done over a trian-  
 461 gulated domain with additional knots in the neighbourhood of the triangle vertices,  
 462 as explained in Section 2. For a point  $\mathbf{x}$  well within the domain (away from the  
 463 triangle edges), the basis functions follow partition of unity and total volume un-  
 464 der the derivative functions is zero (modulo very small approximation errors). But  
 465 when  $\mathbf{x}$  is close to the triangle edges and the knots are too close or far away from the  
 466 vertices, errors creep in computing the basis functions and their derivatives, which  
 467 deviate from the above properties. This high sensitivity of the basis functions to the  
 468 knot placement is consistently observed across the numerical experiments. Shape  
 469 functions via polynomial reproduction are thus consistently adopted to overcome  
 470 this difficulty.

#### 471 4.1.2 Non-polynomial functions

472 Trigonometric and exponential functions, and their derivatives up to the fourth or-  
 473 der are now computed over the same square domain and at the same points as in  
 474 the case of polynomial functions and relative  $L^2$  error norms are tabulated in Table  
 475 4.

476 As expected, we observe from Table 4 that as the functional complexity (say, in  
 477 terms of its departure from polynomials as measured by the number of mono-  
 478 mial bases needed for approximation over an interval) increases, so do the relative  
 479  $L^2$  error norms. To have an understanding of the order of errors involved, plots  
 480 of the exact and approximated fourth order derivatives of the function  $f(x, y) =$   
 481  $\sin(\pi x) \cos(\pi y)$  are given in Fig. 13.

## 482 4.2 Laplace's and Poisson's Equations

The second order Laplace's and Poisson's equations in 2D, often used as workhorse  
 examples for validating new schemes in computational mechanics, are given re-  
 spectively as:

$$\frac{\partial^2 f(x, y)}{\partial x^2} + \frac{\partial^2 f(x, y)}{\partial y^2} = 0 \quad (19)$$

and

$$\frac{\partial^2 f(x, y)}{\partial x^2} + \frac{\partial^2 f(x, y)}{\partial y^2} = g(x, y) \quad (20)$$

Table 2: Relative  $L^2$  error norms of polynomial functions and their derivatives with non-polynomial reproducing (standard) DMS-spline shape functions

$f(x,y)$	$(x+y)$	$(x+y)^2$	$(x+y)^3$	$(x+y)^4$	$(x+y)^5$
$n$	1	2	3	4	5
$N_{nd}$	4	9	16	25	36
$N_e$	2	2	2	2	2
$f - f^{a rel}_{L^2}$	$1.79 \times 10^0$	$3.79 \times 10^0$	$6.08 \times 10^0$	$9.96 \times 10^0$	$1.50 \times 10^1$
$\frac{\partial f}{\partial x} - \left(\frac{\partial f}{\partial x}\right)^{a rel}_{L^2}$	$1.76 \times 10^1$	$2.61 \times 10^1$	$3.57 \times 10^1$	$6.75 \times 10^1$	$9.46 \times 10^1$
$\frac{\partial f}{\partial y} - \left(\frac{\partial f}{\partial y}\right)^{a rel}_{L^2}$	$1.90 \times 10^1$	$2.93 \times 10^1$	$3.28 \times 10^1$	$7.13 \times 10^1$	$9.04 \times 10^1$
$n$	2	3	4	5	6
particles	9	16	25	36	49
triangles	2	2	2	2	2
$f - f^{a rel}_{L^2}$	$1.83 \times 10^0$	$3.43 \times 10^0$	$5.97 \times 10^0$	$9.25 \times 10^0$	$1.44 \times 10^1$
$\frac{\partial f}{\partial x} - \left(\frac{\partial f}{\partial x}\right)^{a rel}_{L^2}$	$1.19 \times 10^1$	$1.86 \times 10^1$	$3.71 \times 10^1$	$5.26 \times 10^1$	$9.40 \times 10^1$
$\frac{\partial f}{\partial y} - \left(\frac{\partial f}{\partial y}\right)^{a rel}_{L^2}$	$1.33 \times 10^1$	$1.64 \times 10^1$	$3.75 \times 10^1$	$4.65 \times 10^1$	$9.97 \times 10^1$
$n$	1	2	3	4	5
particles	16	49	100	169	256
triangles	18	18	18	18	18
$f - f^{a rel}_{L^2}$	$4.18 \times 10^{-1}$	$6.10 \times 10^{-1}$	$9.37 \times 10^0$	$1.35 \times 10^0$	$2.40 \times 10^0$
$\frac{\partial f}{\partial x} - \left(\frac{\partial f}{\partial x}\right)^{a rel}_{L^2}$	$9.17 \times 10^0$	$1.35 \times 10^1$	$2.23 \times 10^1$	$3.89 \times 10^1$	$7.36 \times 10^1$
$\frac{\partial f}{\partial y} - \left(\frac{\partial f}{\partial y}\right)^{a rel}_{L^2}$	$9.22 \times 10^0$	$1.50 \times 10^1$	$2.38 \times 10^1$	$3.58 \times 10^1$	$5.43 \times 10^1$

483 where,  $f(x,y)$  and  $g(x,y)$  are functions in  $\mathbb{R}^2$ . Weak forms of the homogeneous  
 484 Laplace's equation and inhomogeneous Poisson's equation under Dirichlet bound-  
 485 ary conditions are solved via the present scheme over square and triangular do-  
 486 mains.

487 **Square domain**

The square domain (of size  $1 \times 1$ ) is the same as that used in the previous examples. The relative  $L^2$  and  $H^1$  (Sobolev) error norms are computed and tabulated (Table 5). The relative  $H^1$  error norm is defined as:

$$f - f^{a rel}_{H^1} = \frac{\left(\int_{\Omega} \left[ (f - f^a)^2 + (f_{,x} - f^a_{,x})^2 + (f_{,y} - f^a_{,y})^2 \right] d\Omega\right)^{1/2}}{\left(\int_{\Omega} [f^2 + f_{,x}^2 + f_{,y}^2] d\Omega\right)^{1/2}} \quad (21)$$

Table 3: Relative  $L^2$  error norms of polynomial functions and their derivatives with polynomial reproducing DMS-spline based global shape functions

$f(x,y)$	$(x+y)$	$(x+y)^2$	$(x+y)^3$	$(x+y)^4$	$(x+y)^5$
$n$	2	3	4	5	6
$p$	1	2	3	4	5
$N_{nd}$	9	16	25	36	49
$N_e$	2	2	2	2	2
$f - f_{L^2}^{a,rel}$	$2.44 \times 10^{-15}$	$2.47 \times 10^{-13}$	$4.78 \times 10^{-12}$	$9.74 \times 10^{-10}$	$1.23 \times 10^{-7}$
$\frac{\partial f}{\partial x} - \left(\frac{\partial f}{\partial x}\right)_{L^2}^{a,rel}$	$4.13 \times 10^{-15}$	$1.35 \times 10^{-12}$	$9.05 \times 10^{-11}$	$1.14 \times 10^{-8}$	$5.96 \times 10^{-7}$
$\frac{\partial f}{\partial y} - \left(\frac{\partial f}{\partial y}\right)_{L^2}^{a,rel}$	$2.75 \times 10^{-15}$	$4.68 \times 10^{-13}$	$2.23 \times 10^{-11}$	$3.37 \times 10^{-9}$	$5.95 \times 10^{-7}$
$\frac{\partial^2 f}{\partial x^2} - \left(\frac{\partial^2 f}{\partial x^2}\right)_{L^2}^{a,rel}$	-	$2.31 \times 10^{-12}$	$4.26 \times 10^{-10}$	$2.86 \times 10^{-8}$	$4.68 \times 10^{-6}$
$\frac{\partial^2 f}{\partial y^2} - \left(\frac{\partial^2 f}{\partial y^2}\right)_{L^2}^{a,rel}$	-	$3.09 \times 10^{-13}$	$6.21 \times 10^{-11}$	$9.71 \times 10^{-9}$	$3.87 \times 10^{-6}$
$\frac{\partial^2 f}{\partial x \partial y} - \left(\frac{\partial^2 f}{\partial x \partial y}\right)_{L^2}^{a,rel}$	-	$6.45 \times 10^{-13}$	$2.00 \times 10^{-10}$	$1.93 \times 10^{-8}$	$2.97 \times 10^{-7}$
$\frac{\partial^3 f}{\partial x^3} - \left(\frac{\partial^3 f}{\partial x^3}\right)_{L^2}^{a,rel}$	-	-	$5.42 \times 10^{-10}$	$1.29 \times 10^{-7}$	$6.05 \times 10^{-6}$
$\frac{\partial^3 f}{\partial y^3} - \left(\frac{\partial^3 f}{\partial y^3}\right)_{L^2}^{a,rel}$	-	-	$1.68 \times 10^{-10}$	$2.17 \times 10^{-8}$	$4.76 \times 10^{-6}$
$\frac{\partial^4 f}{\partial x^4} - \left(\frac{\partial^4 f}{\partial x^4}\right)_{L^2}^{a,rel}$	-	-	-	$2.94 \times 10^{-7}$	$1.14 \times 10^{-5}$
$\frac{\partial^4 f}{\partial y^4} - \left(\frac{\partial^4 f}{\partial y^4}\right)_{L^2}^{a,rel}$	-	-	-	$1.99 \times 10^{-8}$	$1.70 \times 10^{-5}$
$\frac{\partial^4 f}{\partial x^2 \partial y^2} - \left(\frac{\partial^4 f}{\partial x^2 \partial y^2}\right)_{L^2}^{a,rel}$	-	-	-	$9.09 \times 10^{-8}$	$1.32 \times 10^{-5}$

where ‘ $\partial$ ’ stands for partial differentiation. Presently, the exact solution for Laplace’s equation is given by:

$$f(x,y) = -x^3 - y^3 + 3x^2y + 3xy^2 \quad (22)$$

488 with the trace of the above function on the domain boundary providing the Dirichlet  
489 boundary condition. 3- and 7-point Gauss quadrature rules are used for numerical  
490 integration with  $p = 2$  and  $p = 3, 4$ , respectively. Since derivatives involved in the  
491 relative  $H^1$  error norm are not the primary variables, they are computed at the nodes  
492 with polynomial degree  $p - 1$ . It is clear from the table that, while using  $p = 3$  and  
493 4 considerably reduces the relative  $L^2$  error norm, relative  $H^1$  error norm reduces  
494 substantially with  $p = 4$ . This is clearly due to the fact that the targeted polynomial  
495 function within the domain is of degree 3. For two triangles and 9 nodes, relative  
496  $L^2$  error norm corresponding to  $p = 2$  appears very small owing to 8 out of the 9

Table 4: Relative  $L^2$  error norms of trigonometric and exponential functions and their derivatives

$f(x,y)$	$\sin(xy)$	$\sin(\pi x) \cos(\pi y)$	$e^{(x+y)}$	$e^{(xy)}$
$n$	6	6	6	6
$p$	5	5	5	5
$N_{nd}$	361	361	361	361
$N_e$	18	18	18	18
$f - f^{a\ rel}_{L^2}$	$1.65 \times 10^{-7}$	$4.16 \times 10^{-6}$	$1.03 \times 10^{-7}$	$2.97 \times 10^{-7}$
$\frac{\partial f}{\partial x} - \left(\frac{\partial f}{\partial x}\right)^{a\ rel}_{L^2}$	$9.15 \times 10^{-6}$	$2.79 \times 10^{-4}$	$4.51 \times 10^{-6}$	$1.60 \times 10^{-5}$
$\frac{\partial f}{\partial y} - \left(\frac{\partial f}{\partial y}\right)^{a\ rel}_{L^2}$	$5.17 \times 10^{-6}$	$2.07 \times 10^{-4}$	$1.65 \times 10^{-6}$	$8.43 \times 10^{-6}$
$\frac{\partial^2 f}{\partial x^2} - \left(\frac{\partial^2 f}{\partial x^2}\right)^{a\ rel}_{L^2}$	$3.19 \times 10^{-4}$	$6.89 \times 10^{-3}$	$5.48 \times 10^{-5}$	$5.47 \times 10^{-4}$
$\frac{\partial^2 f}{\partial y^2} - \left(\frac{\partial^2 f}{\partial y^2}\right)^{a\ rel}_{L^2}$	$1.15 \times 10^{-4}$	$5.95 \times 10^{-3}$	$3.05 \times 10^{-5}$	$1.45 \times 10^{-4}$
$\frac{\partial^2 f}{\partial x \partial y} - \left(\frac{\partial^2 f}{\partial x \partial y}\right)^{a\ rel}_{L^2}$	$2.04 \times 10^{-4}$	$3.88 \times 10^{-3}$	$1.89 \times 10^{-5}$	$2.72 \times 10^{-4}$
$\frac{\partial^3 f}{\partial x^3} - \left(\frac{\partial^3 f}{\partial x^3}\right)^{a\ rel}_{L^2}$	$6.61 \times 10^{-3}$	$3.89 \times 10^{-1}$	$2.56 \times 10^{-3}$	$1.61 \times 10^{-2}$
$\frac{\partial^3 f}{\partial y^3} - \left(\frac{\partial^3 f}{\partial y^3}\right)^{a\ rel}_{L^2}$	$3.00 \times 10^{-3}$	$3.05 \times 10^{-1}$	$1.20 \times 10^{-3}$	$7.72 \times 10^{-3}$
$\frac{\partial^4 f}{\partial x^4} - \left(\frac{\partial^4 f}{\partial x^4}\right)^{a\ rel}_{L^2}$	$8.14 \times 10^{-2}$	$1.51 \times 10^{+1}$	$9.59 \times 10^{-2}$	$2.50 \times 10^{-1}$
$\frac{\partial^4 f}{\partial y^4} - \left(\frac{\partial^4 f}{\partial y^4}\right)^{a\ rel}_{L^2}$	$8.29 \times 10^{-2}$	$8.08 \times 10^0$	$5.13 \times 10^{-2}$	$2.05 \times 10^{-1}$
$\frac{\partial^4 f}{\partial x^2 \partial y^2} - \left(\frac{\partial^4 f}{\partial x^2 \partial y^2}\right)^{a\ rel}_{L^2}$	$9.63 \times 10^{-2}$	$7.46 \times 10^0$	$5.03 \times 10^{-2}$	$1.83 \times 10^{-1}$

497 nodes being on the Dirichlet boundary. The plots of error norms are given in Figs.  
 498 14 and 15.

499 Similar results for Poisson’s equation on the square domain are given in Table 6 and  
 500 Fig. 16. If one chooses the solution for Poisson’s equation as:  $f(x,y) = (x+y)^2$ ,  
 501 the forcing function  $g(x,y)$  in equation (20) becomes equal to 4. The relative  $L^2$   
 502 norms for  $n = 2$  and 3 and relative  $H^1$  norm for  $n = 3$  are of the order  $10^{-11}$  even  
 503 with relatively fewer triangles in the triangulation.

504 **Triangular domain**

505 We consider an isosceles triangular domain having base and height equal to unity  
 506 (Fig.17). The error norms (Tables 7 and 8 and Figs. 18 and 19) follow almost  
 507 the same orders as those over the previously adopted square domain. DMS-splines  
 508 with degree 3 gave good results in terms of relative  $L^2$  error norms for solution

Table 5: Relative  $L^2$  and  $H^1$  error norms for different values of  $n$  and  $p$  for the solution of Laplace's equation on a  $1 \times 1$  square domain; exact solution is  $\mathbf{f}(\mathbf{x}, \mathbf{y}) = -\mathbf{x}^3 - \mathbf{y}^3 + 3\mathbf{x}^2\mathbf{y} + 3\mathbf{xy}^2$

$n$	$p$	$N_{nd}$	$N_\varepsilon$	relative $L^2$ norm	relative $H^1$ norm
2	2	9	2	2.6770e-015	8.7596e-001
2	2	49	18	5.4383e-004	3.3199e-001
2	2	85	34	2.3485e-004	2.3802e-001
2	2	105	44	8.8498e-005	1.9596e-001
2	2	133	56	1.0864e-004	1.8392e-001
2	2	149	64	5.8411e-005	1.5327e-001
2	2	189	82	5.8926e-005	1.3130e-001
2	2	253	112	3.3418e-005	1.2021e-001
2	2	321	144	2.0978e-005	1.1105e-001
2	2	513	236	6.6280e-006	8.2411e-002

Table 6: Relative  $L^2$  and  $H^1$  error norms for different values of  $n$  and  $p$  for the solution of Poisson's equation on a  $1 \times 1$  square domain; exact solution is  $\mathbf{f}(\mathbf{x}, \mathbf{y}) = (\mathbf{x} + \mathbf{y})^2$

$n$	$p$	$N_{nd}$	$N_\varepsilon$	relative $L^2$ norm	relative $H^1$ norm
2	2	9	2	1.1085e-015	5.7094e-001
2	2	49	18	2.8673e-015	1.3520e-001
2	2	85	34	2.2191e-015	9.9984e-002
2	2	133	56	3.7470e-015	7.1038e-002
2	2	241	106	4.5526e-015	4.9335e-002
3	3	16	2	1.7116e-012	8.4630e-012
3	3	100	18	1.2748e-012	8.6641e-012
3	3	178	34	9.8971e-013	1.0475e-011
3	3	283	56	1.3155e-012	1.3720e-011
3	3	520	106	1.1802e-012	1.5523e-011

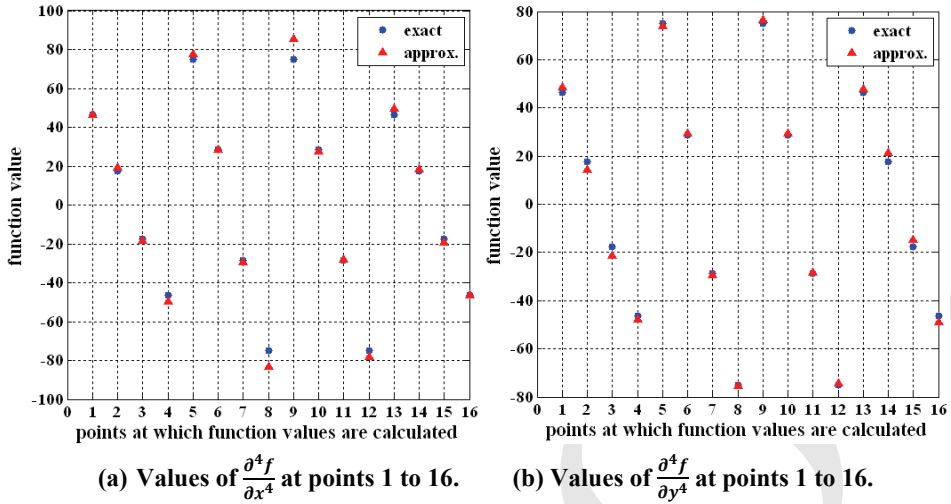


Figure 13: Deviation of approximate values from exact: fourth derivatives of function  $f(x,y) = \sin(\pi x) \cos(\pi y)$

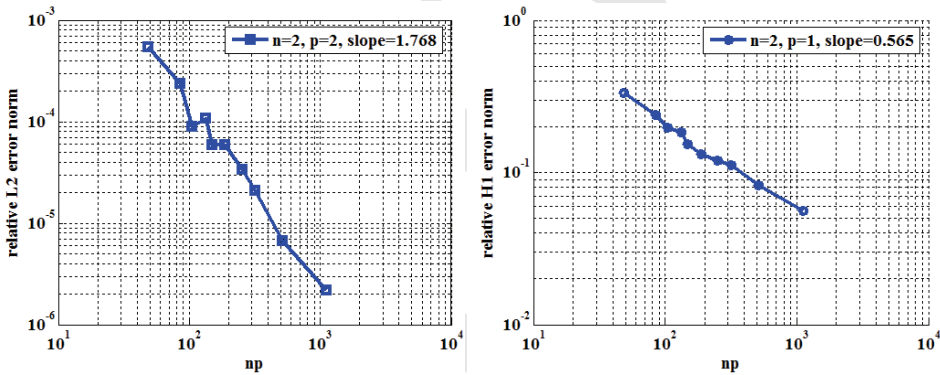


Figure 14: Error plots for solution of Laplace's equation on a square domain with degree of DMS-splines ( $n$ ) = 2 on log-log scale

509 of Laplace's equation with a degree 3 polynomial as the exact solution over both  
 510 square and triangular domains.  $H^1$  error norms are remarkably low with DMS-  
 511 splines of degree 4 (square domain). For Poisson's equation with a second degree  
 512 polynomial as the exact solution, DMS-splines with degree 2 in the approximation  
 513 scheme gave excellent results, as expected, in terms of relative  $L^2$  error norms for  
 514 both domains; however in terms of relative  $H^1$  error norms, degree 3 DMS-splines

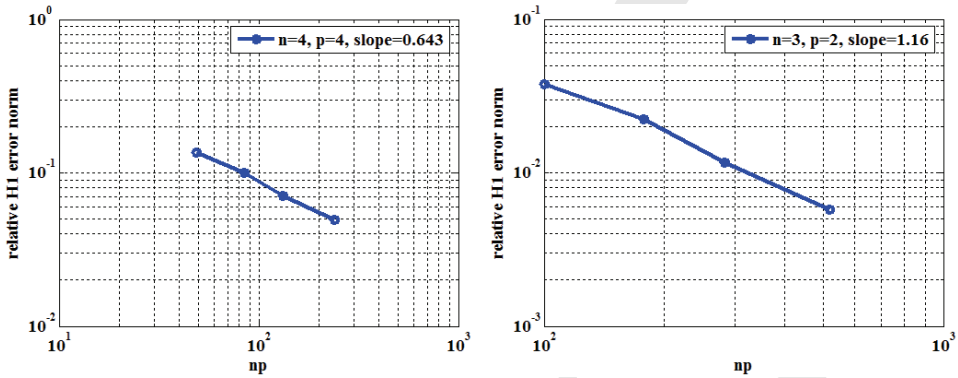


Figure 15:  $H^1$  error plots for solution of Laplace's equation on a square domain with degree of DMS-splines ( $n$ ) = 3 and 4 on log-log scale

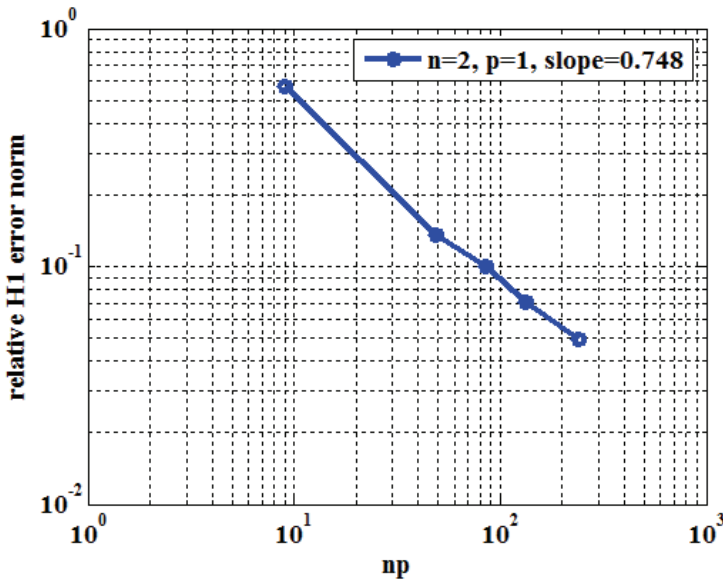


Figure 16:  $H^1$  error plot for solution of Poisson's equation on a square domain with degree of DMS-splines ( $n$ ) = 2 on log-log scale

Table 7: Relative  $L^2$  and  $H^1$  error norms for different values of  $n$  and  $p$  for the solution of Laplace's equation over a triangular domain; exact solution is  $\mathbf{f}(\mathbf{x}, \mathbf{y}) = -\mathbf{x}^3 - \mathbf{y}^3 + 3\mathbf{x}^2\mathbf{y} + 3\mathbf{xy}^2$

$n$	$p$	$N_{nd}$	$N_\epsilon$	relative $L^2$ norm	relative $H^1$ norm
2	2	6	1	0.0000e+000	8.5495e-001
2	2	21	6	9.6275e-004	4.8196e-001
2	2	28	9	1.8471e-004	3.3962e-001
2	2	45	16	6.7271e-005	2.7053e-001
2	2	84	33	7.0390e-005	1.8635e-001
2	2	146	61	3.6987e-005	1.4596e-001
2	2	295	130	1.0125e-005	9.3762e-002
2	2	1059	496	1.1654e-006	4.9086e-002
3	3	10	1	7.7432e-013	4.1871e-001
3	3	55	9	1.5094e-012	4.2113e-002
3	3	91	16	1.5026e-012	2.4358e-002
3	3	121	22	1.7792e-012	2.1451e-002
3	3	166	31	2.1267e-012	1.6027e-002
3	3	175	33	1.7908e-012	1.5216e-002
3	3	310	61	1.8506e-012	6.6388e-003
3	3	637	130	1.8947e-012	3.6726e-003

515 in the approximation scheme perform better in both cases.

516 The motivation for choosing a triangular domain is that it does not admit a bijective  
517 geometric map with a square parametric domain. Hence, if NURBS-based para-  
518 metric bridge method (Shaw *et al.* 2008b) is made use of for the same problem, at  
519 least three sub-domains, each of which is geometrically bijective with the square  
520 parametric domain, must be defined on the triangle and assembly performed to  
521 arrive at the solution. This difficulty is not at all encountered in the DMS-based ap-  
522 proach, which is thus eminently more suited to irregular domain geometries. This  
523 point is further illustrated in some of the examples involving plane stress and plain  
524 strain problems considered in the next section.

### 525 4.3 Plane Stress and Plane Strain Problems

526 First, we consider linear isotropic cases of plane stress and plane strain problems.  
527 Here, we also aim at comparing some of the results with a few other mesh-free  
528 methods and the FEM.

Table 8: Relative  $L^2$  and  $H^1$  error norms for different values of  $n$  and  $p$  for the solution of Poisson's equation on a triangular domain. Exact solution is  $\mathbf{f}(\mathbf{x}, \mathbf{y}) = (\mathbf{x} + \mathbf{y})^2$ .

$n$	$p$	$N_{nd}$	$N_\varepsilon$	relative $L^2$ norm	relative $H^1$ norm
2	2	6	1	0.0000e+000	6.9300e-001
2	2	28	9	1.4187e-015	1.7598e-001
2	2	45	16	1.4928e-015	1.2513e-001
2	2	59	22	2.2053e-015	9.0950e-002
2	2	84	33	1.9395e-015	8.1210e-002
2	2	146	61	1.9862e-015	6.2223e-002
2	2	295	130	1.8111e-015	3.9158e-002
3	3	10	1	3.7988e-013	3.3324e-012
3	3	55	9	1.0115e-012	5.7882e-012
3	3	91	16	1.0443e-012	8.3737e-012
3	3	121	22	1.0979e-012	8.3986e-012
3	3	175	33	1.2309e-012	1.0973e-011
3	3	310	61	1.1232e-012	1.4606e-011

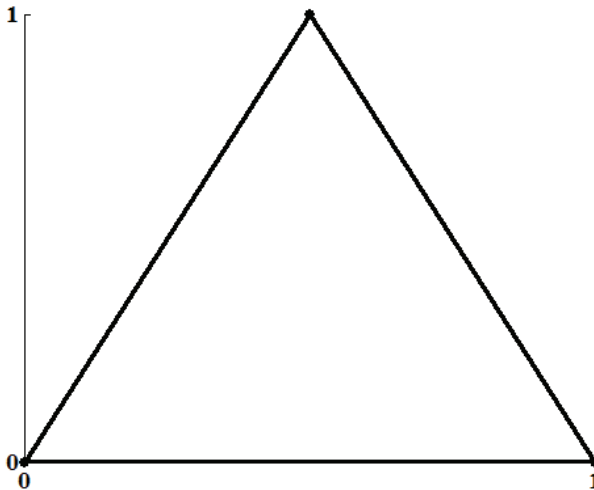


Figure 17: Triangular domain with three particles at its vertices

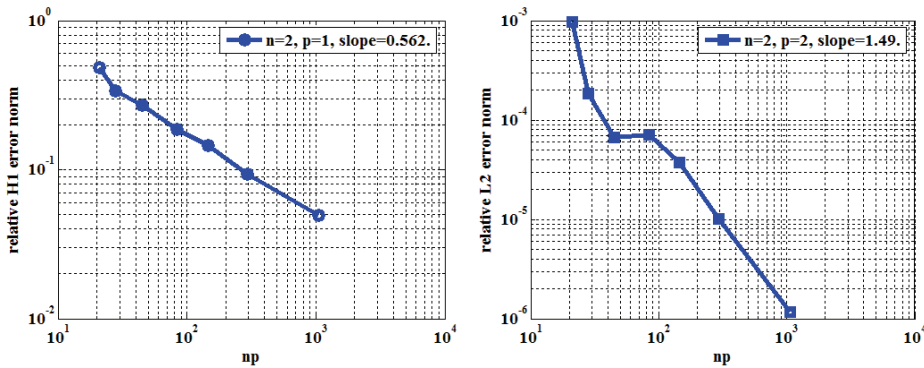


Figure 18: Error plots for solutions of Laplace's equation over a triangular domain with degree of DMS-splines ( $n$ ) = 2 on log-log scale

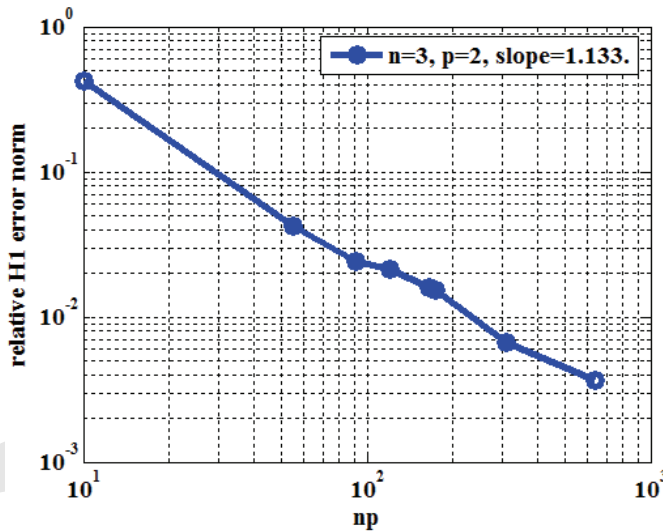


Figure 19:  $H^1$  error plot for solution of Laplace's equation over a triangular domain with degree of DMS-splines ( $n$ ) = 3 on log-log scale

529 4.3.1 Cook's membrane

530 Cook's membrane is one of the benchmark problems in two-dimensional elasticity,  
 531 especially in assessing the performance and robustness of a scheme against possible  
 532 ill-conditioning of the discretized equations. Thus, we consider a skewed plate-like  
 533 structure (of unit thickness) with the planar dimensions as indicated in Fig.20. It

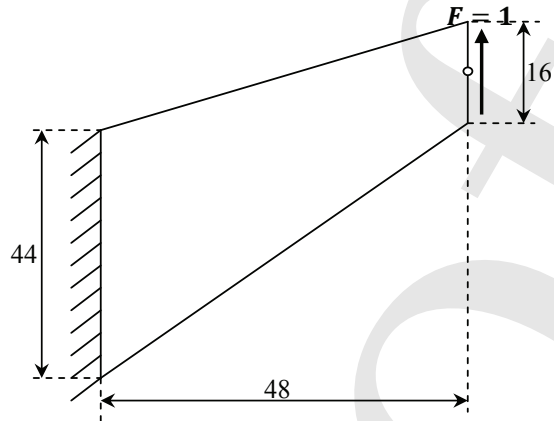


Figure 20: Cook's membrane: the small white circle on its right edge represents the point at which its vertical displacement is computed

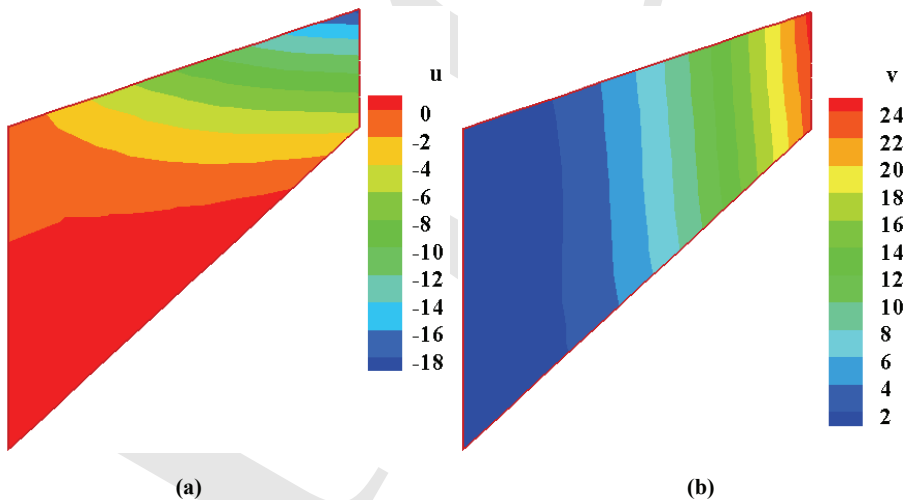


Figure 21: The Cook's membrane with displacement contours; (a)  $x$ -displacement (u), (b)  $y$ -displacement (v)

534 is clamped at one end and a unit shear force is applied at the other. In the plane  
 535 stress case, Young's modulus ( $E$ ) is assumed as unity and Poisson's ratio  $\nu = 0.33$ .  
 536 Vertical deflection of the centre point of its free edge has been reported by many  
 537 authors (such as Simo *et al.* 1989) to be 23.96 (units) as an FEM-based converged  
 538 solution. The deflection contours of the Cook's membrane are shown in Fig.21.  
 539 Comparisons of convergence to the reported solution with those via the RKPM,  
 540 parametric mesh free method, FEM Q4 (4-noded quadrilateral elements), FEM  
 541 T6 (6-noded triangular elements) and, finally, the present scheme are reported in  
 542 Fig.22.

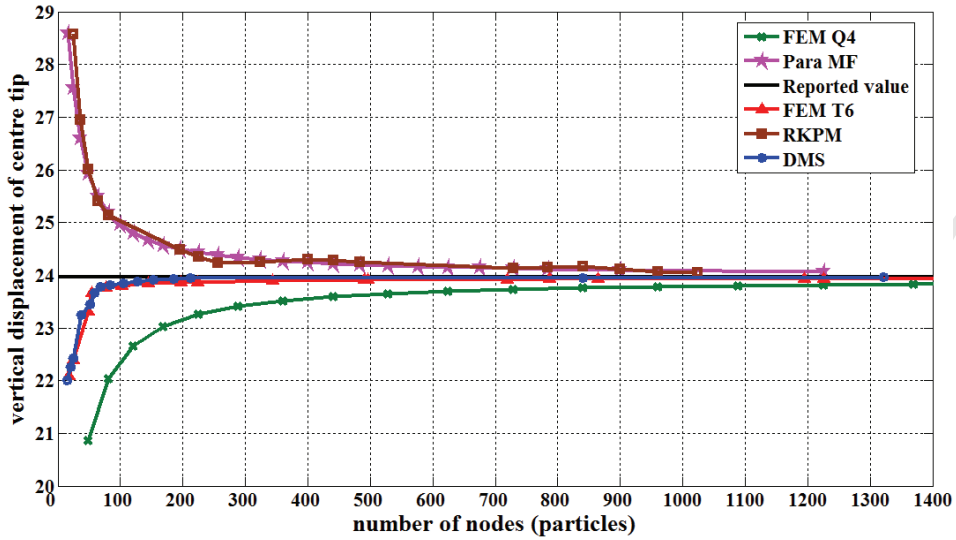
543 As observed, the present scheme approaches the reported value of the vertical dis-  
 544 placement at the centre tip faster than the others. Whereas FEM with Q4 elements,  
 545 NURBS-based parametric mesh-free method and RKPM take more than 1000 par-  
 546 ticles to reach adequately close to the reported value, the present scheme takes just  
 547 about 100 particles to do so. It can be seen from the magnified views (Fig.22(b))  
 548 that the present scheme is even better than FEM T6 in terms of convergence to the  
 549 true solution.

550 A plane strain case is also discussed where the same material and geometric data  
 551 are used except that Poisson's ratio is kept as a variable. The numerical stability of  
 552 the methods as the material approaches the incompressibility limit ( $\nu \rightarrow 0.5$ ) is  
 553 under focus and the results are shown in Fig. 23. Comparable number of particles  
 554 or nodal points (as applicable; about 100 of them) is used with the FEM as well  
 555 as the present scheme. It is seen that the numerical behaviour of FEM T6 and the  
 556 current approach is considerably more stable vis-à-vis FEM Q4 (Figs. 23 and 24).  
 557 Moreover, as seen from the magnified views in Fig.23(b), the present scheme with  
 558 degree 3 DMS-splines behaves better than that with degree 2 DMS-splines.

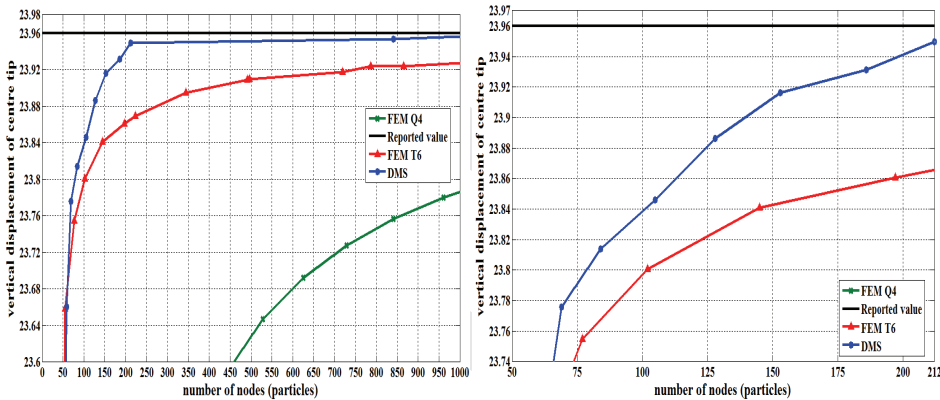
#### 559 4.3.2 An infinite plate with a circular hole

560 Consider an infinite plate with a hole of unit radius, subjected to uniform stretching  
 561 along the (horizontal)  $x$ -direction. A square portion of the plate with the hole at its  
 562 centre and having dimensions 20 times the radius of the hole is considered with the  
 563 assumption that the effect of stress concentration due to the central hole completely  
 564 dies out at the domain boundary. It is known (Timoshenko and Goodier 1934) that  
 565 the stress concentration factor ( $\frac{\sigma_x}{\sigma_b}$ , where  $\sigma_x$  is the normal stress at a point along  
 566 a cross-section of the plate and  $\sigma_b$  is the applied stretching stress at the boundary)  
 567 is 3 at the circumference of the hole (at point A) and reduces quickly towards  
 568 the boundary along the line AB. The following material properties are considered:  
 569  $E = 10000$ ,  $\nu = 0.3$ . The thickness of the plate is assumed to be unity. Quadratic  
 570 DMS-splines are used as kernel functions.

571 Taking advantage of the symmetry of the plate, only one-quarter of it is modelled

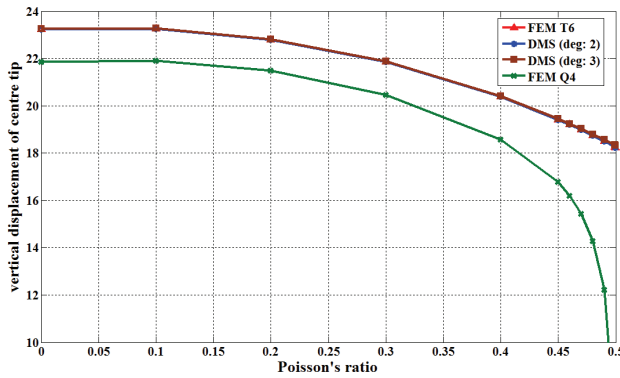


(a)

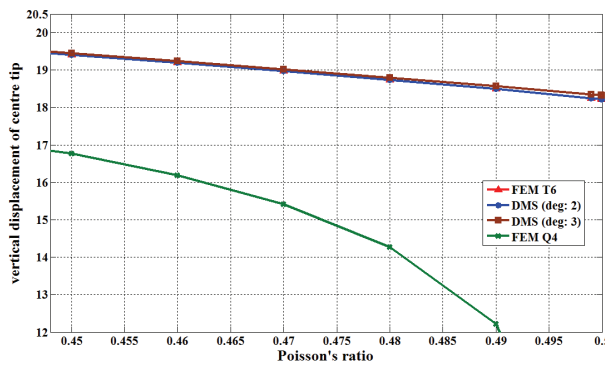


(b)

Figure 22: (a) Comparisons of the performance of different mesh-based and mesh free methods in determining vertical displacement of the centre tip of Cook’s membrane (plane stress problem); (b) Cook’s membrane (plane stress): magnified views depicting the performance of the present scheme and the FEM in determining vertical displacement of the centre tip; faster convergence of the present scheme vis-à-vis FEM with T6 elements is clearer; solution via FEM with Q4 elements is far worse



(a)



(b)

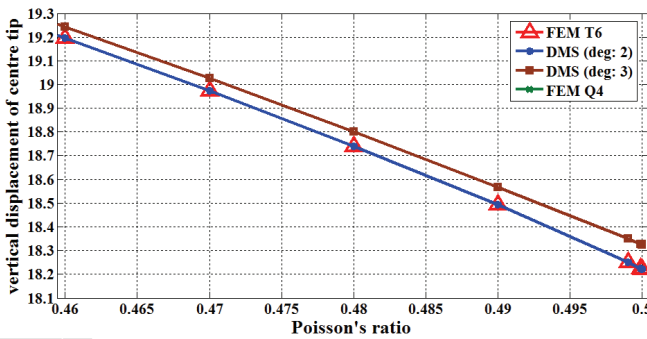


Figure 23: (a) Comparison of the numerical stability of FEM Q4, FEM T6 and DMS-spline global scheme in determining vertical displacement of the centre tip of Cook's membrane as  $\nu \rightarrow 0.5$  (plane strain problem); (b) Comparison of the numerical stability of FEM Q4, FEM T6 and DMS-spline global scheme in determining vertical displacement of the centre tip of Cook's membrane as  $\nu \rightarrow 0.5$  (plane strain problem) - magnified views: degree 3 DMS-splines perform better than second degree DMS-splines and FEM T6 elements

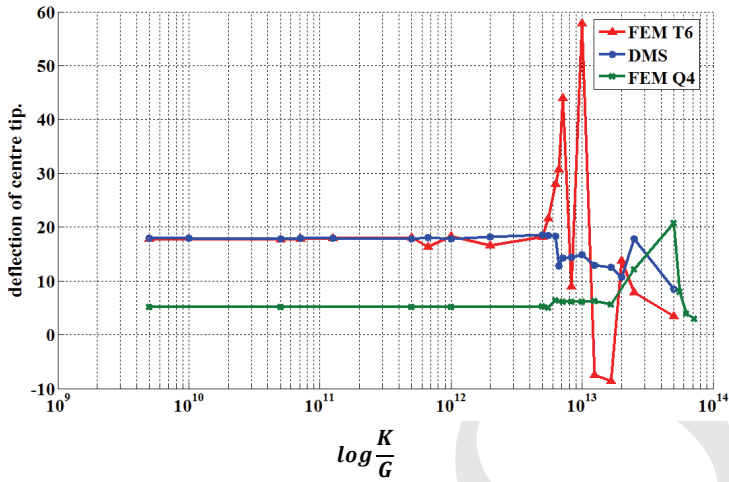


Figure 24: Behaviour of FEM T6, FEM Q4 and DMS-splines based global scheme as  $\nu \rightarrow 0.5$  plotted on a semi-log graph;  $K$  = bulk modulus and  $G$  = Shear modulus

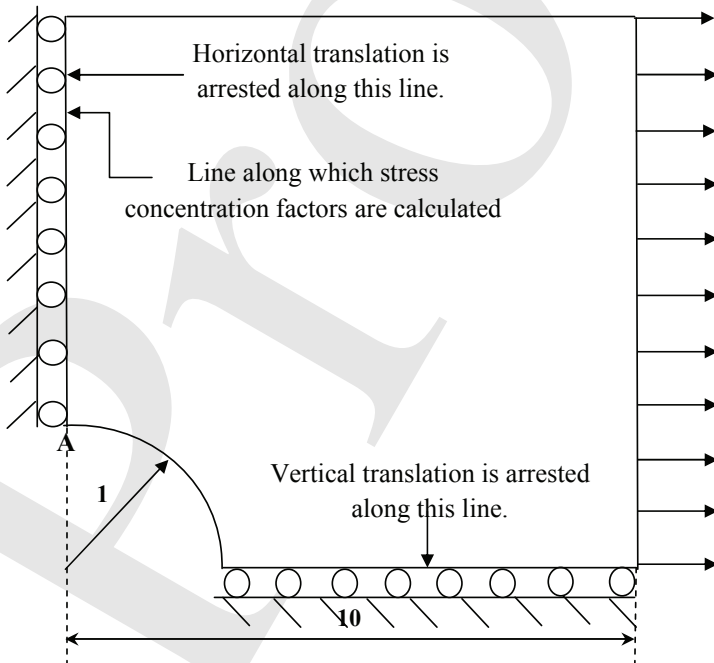


Figure 25: One-quarter of plate with circular hole; Dimensions, boundary conditions and applied stretching force are shown

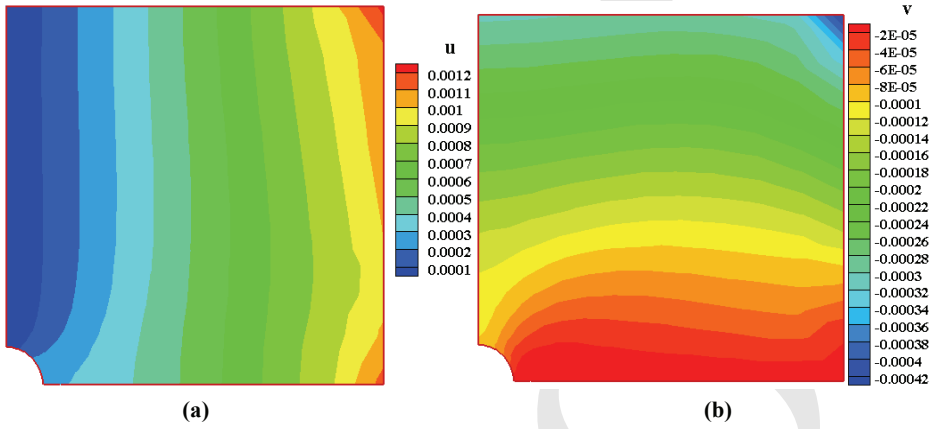


Figure 26: Displacement contours of the plate with circular hole; (a) x-displacement (u), (b) y-displacement (v)

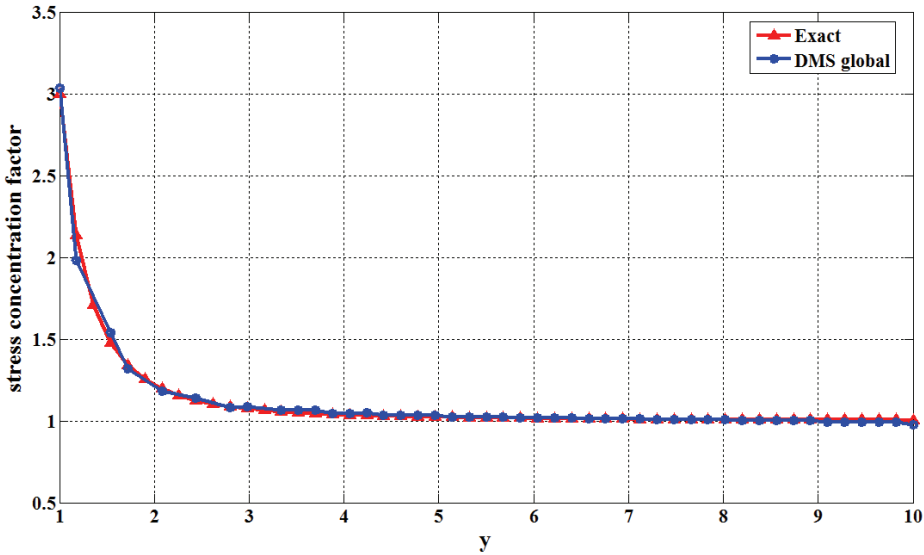


Figure 27: Stress concentration factors plotted along a cross-section (y direction) of the plate

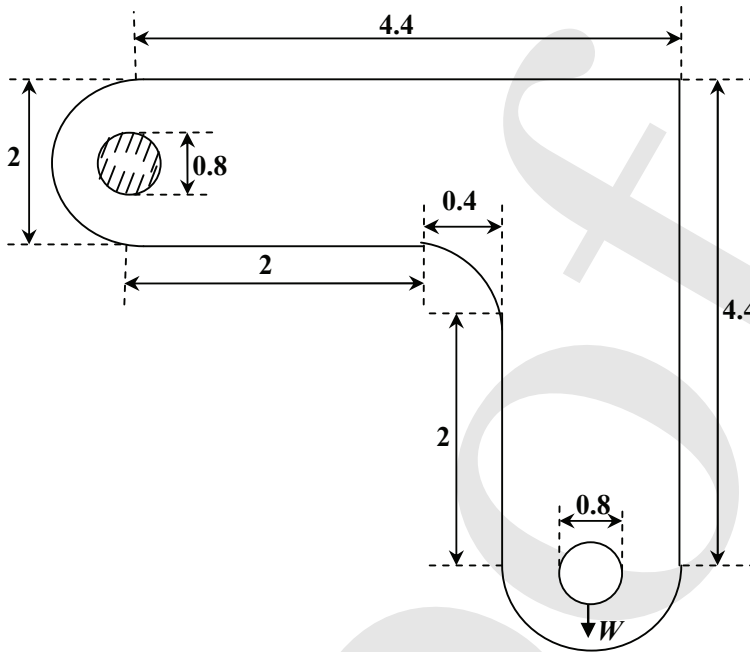


Figure 28: A bracket with dimensions, boundary conditions and concentrated load  $W$

572 for numerical work (Fig.25). The displacement contours of the plate is given in  
 573 Fig.26 and plot of stress concentration factors along a cross-section of the plate  
 574 (line AB in Fig.25) via the present scheme is shown in Fig.27 along with the exact  
 575 solution. Fig.27 shows that the stress concentration factors determined with the  
 576 present approximation scheme are in close agreement with the exact values.

#### 577 4.3.3 A bracket subjected to a concentrated force

578 A two-dimensional bracket as shown in Fig.28 is considered as the final example.  
 579 The dimensions, boundary conditions and application of a concentrated force are  
 580 as shown in the figure. Thickness of the bracket is again taken as unity and the  
 581 material properties are:  $E = 200000$ ,  $\nu = 0.3$ . A concentrated load  $W = 100$  is  
 582 applied as shown in Fig.28. Quadratic DMS-splines are used as kernel functions.  
 583 This example aims at highlighting the advantage (e.g. the algorithmic simplicity)  
 584 of the proposed scheme over the NURBS-based parametric bridge method (Shaw  
 585 *et al.*, 2008b). In the reported results via the latter scheme, the same bracket had  
 586 to be divided into several sub-domains so as to establish a family of bijective geo-  
 587 metric maps between each sub-domain and the parametric domain. The deflection

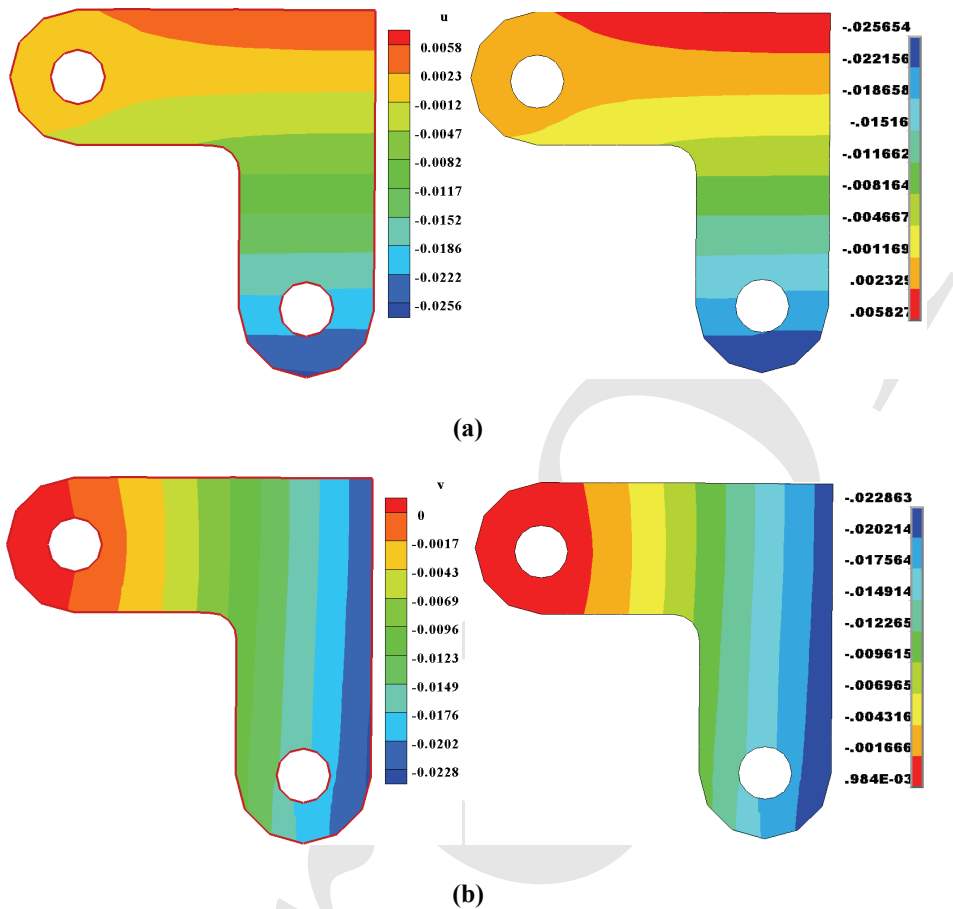


Figure 29: Displacement contours of bracket; results of present method is shown to the left and FEM results (using ANSYS), to the right; (a) x-displacement (u), (b) y-displacement (v)

588 contours of the bracket through the present method and FEM (using ANSYS) are  
 589 shown in Fig.29. The displacements are in good agreement with FEM solutions.

## 590 5 Concluding Remarks

591 This work constitutes a remarkable improvement over an earlier effort to bridge  
 592 the FEM and mesh-free methods based on tensor-product NURBS (Shaw *et al.*  
 593 2008a). The improvement has been arrived at by replacing tensor-product NURBS  
 594 with triangular B-splines (or DMS-splines), constructed over a Delaunay triangu-

595 lation of the domain. This has enabled establishing globally smooth functional  
596 and derivative approximations for general 2D domains (including non-simply con-  
597 nected domains) whilst bypassing a geometric map, which can, potentially, precip-  
598 itate ill-conditioning of the discretized system equations and numerical pollution  
599 of solutions. Thus, while remaining strictly within the conventional domain dis-  
600 cretization of the FEM, one obtains numerically robust and smooth approximations  
601 to the target function and its derivatives across element boundaries – a characteristic  
602 feature of mesh-free methods. The numerical robustness of the present functional  
603 approximation is however dependent crucially upon an admissible placement of  
604 knots around the triangle vertices and using a polynomial reproduction step while  
605 generating the shape functions. While the generation of knotclouds near the ver-  
606 tices of triangles is carefully done so as to strictly satisfy the non-collinearity of any  
607 three knots fall, the latter ploy involving polynomial reproduction is, in particular,  
608 shown to remarkably reduce the sensitive dependence of the approximant to small  
609 (and admissible) variations in the knot locations. The polynomials reproduced are  
610 of degree  $p \leq n$ , where  $n$  is the degree of DMS-splines. The shape functions so gen-  
611 erated are  $C^{n-1}$  across triangle boundaries. Unlike the NURBS-based parametric  
612 bridge method, which was a precursor to this development, the nodes presently do  
613 not double up as knots and this prevents possible misalignment of background cells  
614 (i.e., the triangles themselves) with the supports of shape functions (irrespective of  
615 the degree of the employed DMS-splines) while applying the scheme to the weak  
616 form of the governing equations. Some of the advantages of the proposed scheme  
617 are brought out through a number of appropriately chosen numerical examples that  
618 include, among others, the Cook’s membrane problem and a few boundary value  
619 problems defined over non-simply connected domains in 2D.

620 DMS-splines are being increasingly used for solid modelling in the computer graph-  
621 ics literature (Gang Xu, *et al.*, 2008, Yunhao *et al.*, 2007). Given the importance of  
622 solid modelling in the pre-processor of every commercial finite element code and  
623 the potential of DMS splines in this respect, the present scheme assumes a sense of  
624 timeliness as it offers a seamless interface between solid modelling and basic FE-  
625 based computing. This could be particularly helpful if the need arises for repeated  
626 re-meshing during a possible  $h$ - $p$  refinement.

627 Further investigations on the method are currently under progress. These include  
628 a-priori and a-posteriori error estimates, extension to 3D domains and applications  
629 to problems involving material and geometric non-linearity. Of specific interest in  
630 the last category are the problems of simulating ultra-thin membranes and plates  
631 developing shear bands. Some of these results would soon be reported elsewhere.

632 **References**

- 633 **Ainsworth M.; Coggins P.** (2000): The stability of mixed *hp* finite element meth-  
634 ods for Stokes flow on high aspect ratio elements, *SIAM. Journal of Numerical*  
635 *Analysis*, Vol. 38, pp.1721-1761.
- 636 **Atluri S. N.; Zhu T.** (1998): A new meshless local Petrov-Galerkin (MLPG) ap-  
637 proach in computational mechanics, *Computational Mechanics*, Vol. 22, pp.117-  
638 127.
- 639 **Atluri S. N.; Zhu T.** (2000): The meshless local Petrov-Galerkin (MLPG) ap-  
640 proach for solving problems in elasto-statics, *Computational Mechanics*, Vol. 25,  
641 pp.169-179.
- 642 **Atluri S. N.; Han Z. D.; Rajendran A. M.** (2004): A new implementation of the  
643 meshless finite volume method, through MLPG mixed approach, *CMES: Computer*  
644 *Modelling in Engineering and Sciences*, Vol. 6, no.6, pp.491-513.
- 645 **Atluri S. N.; Kim H. G.; Cho J. Y.** (1999): A critical assessment of the truly  
646 Meshless local Petrov-Galerkin (MLPG) methods, *Computational Mechanics*, Vol.  
647 24, pp. 348-372.
- 648 **Atluri S. N.; Sladek J.; Sladek V.; Zhu T.** (2000): The local boundary integral  
649 equation (LBIE) and it's meshless implementation for linear elasticity, *Computa-*  
650 *tional Mechanics*, Vol. 25, pp.180-198.
- 651 **Atluri, S. N.; Liu H. T.; Han Z. D.** (2006a): Meshless local Petrov-Galerkin  
652 (MLPG) mixed collocation method for elasticity problems, *CMES: Computer Mod-*  
653 *elling in Engineering and Sciences*, Vol. 14, no.3, pp.141-152.
- 654 **Atluri, S. N.; Liu H. T.; Han Z. D.** (2006b): Meshless local Petrov-Galerkin  
655 (MLPG) mixed finite difference method for solid mechanics, *CMES: Computer*  
656 *Modelling in Engineering and Sciences*, Vol. 15, no.1, pp.1-16.
- 657 **Auricchio F.; Beirao da Veiga L.; Lovadina C.; Reali A.** (2005): A stability study  
658 of some mixed finite elements for large deformation elasticity problems, *Computer*  
659 *Methods in Applied Mechanics and Engineering*, Vol. 194, pp.1075-1092.
- 660 **Babuška I.; Melenk J. M.** (1997): The partition of unity method, *International*  
661 *Journal of Numerical Methods in Engineering*, Vol. 40, pp.727-758.
- 662 **Belytschko T.; Lu Y. Y.; Gu L.** (1994): Element-free Galerkin methods, *Internat-*  
663 *ional Journal of Numerical Methods in Engineering*, Vol. 37, pp.229-256.
- 664 **Cai Y. C.; Zhu H. H.** (2004): Direct imposition of essential boundary conditions  
665 and treatment of material discontinuities in the EFG. method, *Computational Me-*  
666 *chanics*, Vol. 34, pp.330-338.
- 667 **Dahmen W.; Micchelli C. A.; Seidel H. P.** (1992): Blossoming begets B-splines

- 668 built better by B-patches, *Mathematics of computation*, Vol. 59, no. 199, pp.97-  
669 115.
- 670 **Duarte C. A.; Oden J. T.** (1997): An h-p adaptive method using clouds, *Computer*  
671 *Methods in Applied Mechanics and Engineering*, Vol. 139, pp.237-262.
- 672 **Engel G.; Garikipati K.; Hughes T. J. R.; Larson M. G.; Mazzei L.; Taylor**  
673 **R. L.** (2002): Continuous/discontinuous finite element approximations of fourth  
674 order elliptic problems in structural and continuum mechanics with applications to  
675 thin beams and plates, and strain-gradient elasticity, *Computer Methods in Applied*  
676 *Mechanics and Engineering*, Vol. 191, pp.3669-3750.
- 677 **Fong P.; Seidel H.** (1993): An implementation of triangular B-spline surfaces over  
678 arbitrary triangulations, *Computer Aided Geometric Design*, Vol. 10, pp.267-275.
- 679 **Franssen M. G. J.** (1995): *Evaluation of DMS-splines*, Masters thesis, Department  
680 of Mathematics and Computing science, Eindhoven university of technology.
- 681 **Gamallo P.; Astley R. J.** (2007): A comparison of two Trefftz-type methods: the  
682 ultraweak variational formulation and the least square method, for solving short-  
683 wave 2-D Helmholtz problems, *International Journal for Numerical Methods in*  
684 *Engineering*, Vol. 71, pp.406-432.
- 685 **Gang Xu; Guo-Zhao Wang; Xiao-Diao Chen** (2008): Free-form deformations  
686 with rational DMS-spline volumes, *Journal of Computer Science and Technology*,  
687 Vol. 23(5), pp.862-873.
- 688 **Gingold R. A.; Monaghan J. J.** (1977): Smoothed particle hydrodynamics: theory  
689 and application to non-spherical stars, *Monthly Notices of the Royal Astronomical*  
690 *Society*, Vol. 181, pp.275-389.
- 691 **Han W.; Meng X.** (2001): Error analysis of the reproducing kernel particle method,  
692 *Computer Methods in Applied Mechanics in Engineering*, Vol. 190, pp.6157-6181.
- 693 **Hughes T. J. R.** (1995): Multiscale phenomena: Green's functions, the Dirichlet-  
694 to-Neumann formulation, subgrid scale models, bubbles and the origins of sta-  
695 bilized methods, *Computer methods in applied mechanics and engineering*, 127,  
696 pp.387-401.
- 697 **Hughes T. J. R.; Guglielmo Scovazzi; Leopoldo P. Franca** (2004): *Multiscale*  
698 *and stabilized methods*, Encyclopaedia of computational mechanics, John Wiley &  
699 sons, ltd.
- 700 **Kita Eisuke; Kamiya Norio** (1995): Trefftz method: an overview, *Advances in*  
701 *Engineering Software*, 24, pp.3-12.
- 702 **Liu W. K.; Jun S.; Zhang Y. F.** (1995a): Reproducing kernel particle methods,  
703 *International Journal for Numerical Methods in Fluids*, Vol. 20, pp.1081-1106.
- 704 **Liu W. K.; Jun S.; Li S.; Adee J.; Belytschko T.** (1995b): Reproducing ker-

- 705 nel particle methods for structural dynamics, *International Journal for Numerical*  
706 *Methods in Engineering*, Vol. 38, pp.1655-1679.
- 707 **Liu W. K.; Li S.; Belytschko T.** (1997): Moving least square reproducing kernel  
708 methods (I) methodology and convergence, *Computer Methods in Applied Mechan-*  
709 *ics and Engineering*, Vol. 143, pp.113-154.
- 710 **Lucy L. B.** (1977): A numerical approach to the testing of the fission hypothesis,  
711 *The Astronomical Journal*, Vol. 82, pp.1013-1024.
- 712 **Micchelli C. A.** (1995): Mathematical aspects of geometric modelling, In: *CBMS-*  
713 *NSF regional conference series in applied mathematics*, vol. 65. Philadelphia, PA:  
714 SIAM.
- 715 **Nayroles B.; Touzot G.; Villon P.** (1992): Generalizing the finite element method:  
716 diffuse approximation and diffuse elements, *Computational Mechanics*, Vol. 10,  
717 pp.307-318.
- 718 **Onate E.; Valls A.; Garcia J.** (2006): FIC/FEM formulation with matrix stabi-  
719 lizing terms for incompressible flows at low and high Reynolds numbers, *Comput.*  
720 *Mech.*, 38, pp.440-455.
- 721 **Pfeifle; Seidel H. P.** (1994): Faster evaluation of quadratic bivariate DMS-spline  
722 surfaces, *Canadian Human Computer Communications Society Graphics Interface*,  
723 pp.182-190.
- 724 **Shaw A.; Roy D.** (2007a): A NURBS-based Error Reproducing Kernel Method  
725 with Applications in Solid Mechanics, *Computational Mechanics*, Vol. 40, pp.127-  
726 148.
- 727 **Shaw A.; Roy D.** (2008a): NURBS-based Parametric Mesh-free Methods, *Com-*  
728 *puter methods in applied mechanics and engineering*, Vol. 197, pp.1541-1567.
- 729 **Shaw A.; Banerjee, B.; Roy D.** (2008b): A NURBS-based parametric method  
730 bridging mesh free and finite element formulations, *CMES: Computer Modelling*  
731 *in Engineering and Sciences*, Vol. 26(1), pp.31-35.
- 732 **Shaw A.; Bendapudi S.; Roy D.** (2008c): A Kriging-based Error Reproducing  
733 and Interpolating Kernel Method for Improved Mesh-free Approximations, *Inter-*  
734 *national Journal for Numerical Methods in Engineering*, Vol. 73, pp.1434-1467.
- 735 **Shuyao Long; Atluri S. N.** (2002): A. meshless local Petrov-Galerkin method  
736 for solving the bending problem of a thin plate, *CMES: Computer Modelling in*  
737 *Engineering and Sciences*, Vol. 3(1), pp.53-63.
- 738 **Simo, J. C.; Fox D. D.; Rifai M. S.** (1989): On a stress resultant geometrically ex-  
739 act shell model: Part II-The linear theory; computational aspects, *Computer meth-*  
740 *ods in applied mechanics and engineering*, Vol. 73, pp.53-92.
- 741 **Sonia Fernandez-Mendez; Antonio Huerta** (2004): Imposing essential boundary

- 742 conditions in mesh-free methods, *Computer Methods in Applied Mechanics and*  
743 *Engineering*, Vol. 193, pp1257-1275.
- 744 **Soric J.; Jarak T.** (2010): Mixed meshless formulation for analysis of shell-like  
745 structures, *Computer Methods in Applied Mechanics and Engineering*, Vol. 199,  
746 pp. 1153-1164.
- 747 **Timoshenko S. P.; Goodier, J. N.** (1934): *Theory of elasticity*, McGrawhill inter-  
748 national editions.
- 749 **Yunhao Tan; Jing Hua; Ming Dong** (2007): 3D reconstruction from 2D images  
750 with hierarchical continuous simplices, *The Visual Computer*, Vol. 23, pp.905-914.
- 751 **Zhu T.; Atluri, S. N.** (1998): A modified collocation method and a penalty formu-  
752 lation for enforcing the essential boundary conditions in the element free Galerkin  
753 method, *Computational Mechanics*, Vol. 21, pp.211-222.
- 754 **Zhu T.; Zhang J.; Atluri S. N.** (1998): A meshless local boundary integral equa-  
755 tion (LBIE) method for solving nonlinear problems, *Computational Mechanics*,  
756 Vol. 22, pp.174-186.
- 757 **Zienkiwicz, O. C.; Taylor, R. L.; Zhu J. Z.** (1967): *The finite element method: Its*  
758 *basis and fundamentals*, McGraw-Hill Publishers.

Proof